haematologica
Journal of the Ferrata Storti Foundation

KLF4 overexpression protects against complement-mediated endothelial injury in transplant-associated thrombotic microangiopathy

by Shuhui Jiang, Jiaqian Qi, Tingting Pan, Zhenzhen Yao, Siyi Lu, Yifei Han, Depei Wu and Yue Han

Received: March 4, 2025.
Accepted: July 22, 2025.

Citation: Shuhui Jiang, Jiaqian Qi, Tingting Pan, Zhenzhen Yao, Siyi Lu, Yifei Han, Depei Wu and Yue Han. KLF4 overexpression protects against complement-mediated endothelial injury in transplant-associated thrombotic microangiopathy.
Haematologica. 2025 Aug 7. doi: 10.3324/haematol.2025.287676 [Epub ahead of print]

Publisher's Disclaimer.
E-publishing ahead of print is increasingly important for the rapid dissemination of science. Haematologica is, therefore, E-publishing PDF files of an early version of manuscripts that have completed a regular peer review and have been accepted for publication.
E-publishing of this PDF file has been approved by the authors.
After having E-published Ahead of Print, manuscripts will then undergo technical and English editing, typesetting, proof correction and be presented for the authors' final approval; the final version of the manuscript will then appear in a regular issue of the journal.
All legal disclaimers that apply to the journal also pertain to this production process.

KLF4 overexpression protects against complement-mediated endothelial injury in transplant-associated thrombotic microangiopathy

*Shuhui Jiang[1,2,3], *Jiaqian Qi[1,2,3], *Tingting Pan[1,2,3], Zhenzhen Yao[1,2,3], Siyi Lu[1,2,3], Yifei Han[1,2,3], #Depei Wu[1,2,3,4], #Yue Han[1,2,3,4]

1.National Clinical Research Center for Hematologic Diseases, Jiangsu Institute of Hematology, The First Affiliated Hospital of Soochow University, Suzhou, China.

2.Institute of Blood and Marrow Transplantation, Collaborative Innovation Center of Hematology, Soochow University, Suzhou, China.

3.Key Laboratory of Thrombosis and Hemostasis of Ministry of Heath, Suzhou, China.

4.State Key Laboratory of Radiation Medicine and Protection, Soochow University, Suzhou, China.

*These authors contributed equally to the research.

#Corresponding author:

Depei Wu, MD, PhD.

Address: Jiangsu Institute of Hematology, The First Affiliated Hospital of Soochow University, 188, Shizi Street, Suzhou, Jiangsu Province, 215006, China.

E-mail: drwudepei@163.com

Yue Han, MD, PhD.

Address: Jiangsu Institute of Hematology, The First Affiliated Hospital of Soochow University, 188, Shizi Street, Suzhou, Jiangsu Province, 215006, China.

E-mail: hanyue@suda.edu.cn

Short title: Up-regulation of KLF4 ameliorates TA-TMA

Keywords: hematopoietic stem cell transplantation, thrombotic microangiopathy, KLF4, complement activation, endothelial injury, CD46

Availability of data and material

All original data and code generated or used during the study are available from the corresponding author if necessary. Additional methodological details are provided in the supplementary materials.

Ethics statement

This study involving human participants was approved by the Ethics Committee of the First Affiliated Hospital of Soochow University. Written informed consent was obtained from all participants. The animal protocol was reviewed and approved by the Ethics Committee of Soochow University.

Funding statement

This work was supported by the National Natural Science Foundation of China (82230005,

82200133, 82200137 and 82070143), grants from the Jiangsu Province of China (BE2021645) and the Priority Academic Program Development of Jiangsu Higher Education Institutions (PAPD).

Author contributions

SJ designed and performed research studies, analyzed the data, and wrote the manuscript. JQ and TP performed research studies and analyzed data. ZY, SL and YFH contributed to the collection of clinical data. DW and YH contributed to the research design, data analysis and supervision of the study. SJ, JQ and TP are co-first author; authorship order reflects the degree to which authors drove key developments in the work. All authors contributed to the article and approved the submitted version.

Conflict of interest

The authors declare no conflict of interest.

Abstract word count: 247

Text word count: 4000

Number of figures & tables: 8

Supplementary materials: Tables S1-4; Figures S1-7; supplemental methods

Abstract

Transplant-associated thrombotic microangiopathy (TA-TMA) is a severe complication of hematopoietic stem cell transplantation, marked by excessive complement activation, endothelial injury, and microangiopathy. Although complement blockade benefits some patients, effective prophylactic and therapeutic strategies remain scarce. Therefore, plasma samples from 20 TA-TMA patients and 1:1 matched control patients (matched by age, sex, underlying diagnosis, HLA compatibility, graft source, and donor–recipient ABO blood type) were measured for krüppel-like factor 4 (KLF4), complement proteins and endothelial injury markers. The mechanism was investigated both in vitro and in vivo. In this study, plasma analysis revealed that TA-TMA patients exhibit notably lower KLF4 levels compared to matched controls, as well as elevated endothelial injury markers. In vitro, increased KLF4 expression in human umbilical vein endothelial cells significantly reduced complement deposition and mitigated endothelial damage induced by TA-TMA plasma. Furthermore, KLF4 overexpression notably decreased apoptosis and preserved endothelial barrier integrity. In a mouse model of TA-TMA triggered by dimethyloxalylglycine, upregulation of KLF4 alleviated anemia, thrombocytopenia, and renal complement deposition, while diminishing endothelial inflammatory and thrombotic markers. Intriguingly, pravastatin treatment produced similar improvements. Mechanistic analyses using CUT&Tag, RNA sequencing, luciferase assays, and quantitative real-time PCR revealed that KLF4 binds to the *CD46* promoter, enhancing its transcription and thus restraining complement activation in endothelial cells. These results identify KLF4 as a key negative regulator of complement-mediated endothelial injury in TA-TMA. This

conclusion is supported by CD46 knockdown abolishing KLF4-mediated benefits, highlighting the therapeutic potential of targeting KLF4 or its downstream effectors, including CD46.

Introduction

Transplant-associated thrombotic microangiopathy (TA-TMA), a microangiopathy complicating hematopoietic stem cell transplantation (HSCT), manifests as hemolytic anemia, thrombocytopenia, and organ dysfunction.[1] Because post-transplant renal biopsy carries significant risk, TA-TMA is usually diagnosed clinically and most often manifests 22–100 days after HSCT; consequently, reported incidence varies widely (0.8%–36%).[2] Although certain medications (e.g., calcineurin inhibitors), immune reactions (e.g., graft-versus-host disease), or infectious complications have been implicated, the precise pathophysiology remains under investigation.[3] The recently proposed three-hit model outlines sequential triggers: (1) pre-existing complement or endothelial vulnerability, (2) conditioning-regimen-induced endothelial injury, and (3) additional cumulative insults that together activate the complement cascade and drive microthrombus formation.[4] Increasing evidence suggests that complement dysregulation is central to TA-TMA pathogenesis.[1, 5, 6] Patients carrying complement-gene mutations—and recipients of grafts harboring TMA-associated variants—have an increased risk of TA-TMA,[6, 7] underscoring the value of pre-HSCT genetic screening. In HSCT recipients, activation of the classical and alternative complement pathways causes C5b-9 deposition and subsequent endothelial injury.[6, 8, 9] Management of high-risk TA-TMA currently combines optimized supportive care with complement inhibitors such as eculizumab and narsoplimab, while next-generation agents (ravulizumab, coversin) are undergoing clinical evaluation.[10-13] However, despite improved survival, mortality rates still exceed 30%,[14, 15] and survivors often endure chronic kidney disease,[16] persistent neurological sequelae.[17]

Endothelial cells (ECs), critical regulators of vascular homeostasis, suffer multi-factorial injury during HSCT, including conditioning regimens, infections, circulating cytokines, and complement activation.[18] Indeed, TA-TMA patients exhibit elevated serum levels of endothelial injury markers, including vascular cell adhesion molecule-1 (VCAM-1), plasminogen activator inhibitor-1 (PAI-1), and suppression of tumorigenicity 2 (ST2).[19-21] Since endothelial activation precedes immune and complement responses, EC protection warrants therapeutic prioritization in TA-TMA.[22] Krüppel-like factor 4 (KLF4) is a zinc-finger transcription factor with anti-inflammatory, antithrombotic, and vasodilatory effects in vasculature.[23, 24] Previous studies have shown that KLF4 regulates endothelial transcripts—*endothelial nitric oxide synthase*, *thrombomodulin* (*THBD*), and *PAI-1*[23] —and also governs the membrane-bound regulator *CD55* in both intestinal epithelial cells[25] and human umbilical vein endothelial cells (HUVECs).[26] Notably, EC-specific KLF4 overexpression in mice confers antiadhesive, antithrombotic phenotypes[24] and protects against ischemic acute kidney injury (AKI).[27] Defining KLF4's role in TA-TMA endothelial injury could enable novel prophylaxis.

Our earlier work revealed elevated plasma C3b/C5b-9[28] and *hypoxia-inducible factor-1α* (*HIF-1α*) mRNA in TA-TMA patients versus other HSCT complications, prompting HIF-1α investigation via dimethyloxalylglycine-induced (DMOG) hypoxia–complement injury model.[29] In this study, KLF4 expression was markedly reduced in TA-TMA patients relative to controls, inversely correlating with endothelial-injury markers. To define KLF4's role, we

combined in-vitro and in-vivo approaches. Overexpressing KLF4 in HUVECs curtailed complement deposition and mitigated endothelial damage triggered by TA-TMA plasma, whereas KLF4 upregulation in vivo attenuated key TA-TMA manifestations. Mechanistic analyses—CUT&Tag, bulk RNA-seq, luciferase reporter assays, and quantitative real-time PCR (qPCR)—implicate CD46 as a critical downstream effector, because CD46 knockdown abolished KLF4-mediated benefits.

Methods

Patients

We retrospectively reviewed 2387 patients who underwent allogeneic hematopoietic stem cell transplantation (allo-HSCT) at the First Affiliated Hospital of Soochow University from June 2021 to June 2024. Among them, 20 patients were diagnosed with TA-TMA according to previously published criteria (summarized in supplemental methods).[2] Using 1:1 propensity-score matching for age, sex, underlying diagnosis, HLA compatibility, graft source, and donor–recipient ABO blood type, we identified 20 matched controls from the remaining transplant recipients (Table 1). Within the TA-TMA cohort, five patients developed acute graft-versus-host disease (aGVHD)—one grade I, one grade II, two grade III, and one grade IV—and five had concurrent active infections. In the matched-control cohort, aGVHD occurred in four patients (two grade I, one grade II, and one grade III), and four presented with active infections. EDTA-K_2-anticoagulated plasma from the TA-TMA group was collected at diagnosis, whereas control samples were obtained at a median of 44 days post-transplant. Comprehensive clinical and laboratory

data at sample collection are summarized in Table S1. Additional information on patient measurements is provided in the supplementary methods.

Cell model

HUVECs were maintained at 37°C in 5% CO_2 in Dulbecco's modified Eagle's medium (DMEM) supplemented with 10% fetal bovine serum (Sigma-Aldrich, #F0193) and 1% penicillin/streptomycin (Invitrogen, #15140122). Once cultures reached ~70% confluence, the medium was replaced with DMEM containing 10% plasma from TA-TMA patients or matched controls and incubated for 24 h, thereby establishing an in vitro complement-adherent endothelial-cell model. Comprehensive descriptions of the cell experiments are reported in the supplementary methods.

Animal model

The murine allogeneic HSCT model was first established as described in the Supplementary methods. To induce a TA-TMA–like phenotype in vivo, we used a DMOG-based model previously described by our group. Specifically, DMOG (800 mg/kg body weight; MCE, #HY-15893) or vehicle control (0.9% saline) was administered intraperitoneally once daily for two consecutive days from day 15 post–allo-HSCT. Comprehensive protocols for all additional interventions—including administration of the KLF4 activator APTO-253, in vivo KLF4 over-expression, and pravastatin treatment regimens—are also detailed in the supplementary methods.

Statistics

The statistical analyses are described in the supplementary methods.

Study approval

All research programs comply with the guidelines of the Ethics Committee of the First Affiliated Hospital of Soochow University and adhere to the Declaration of Helsinki.

Results

KLF4 levels and markers of complement activation and endothelial injury in patients with TA-TMA

We first measured plasma levels of complement components and inflammatory/thrombotic endothelial markers. Compared with matched controls, TA-TMA patients exhibited markedly higher concentrations of C3b (473.0 ± 202.1 vs. 165.8 ± 92.6 ng/mL; $p < 0.0001$) (Figure 1A, left), soluble C5b-9 (1139 [754.1–1461] vs. 485.3 [443.0–564.3] ng/mL; $p < 0.0001$) (Figure 1A, center), and ICAM-1 (110.2 [89.6–157.7] vs. 92.8 [81.1–121.9] ng/mL; $p < 0.05$) (Figure 1A, right). Similar increases were noted for VCAM-1 (892.5 [832.7–920.7] vs. 698.1 [455.4–909.8] ng/mL; $p < 0.001$), PAI-1 (133.3 [73.2–290.9] vs. 61.9 [44.9–99.0] ng/mL; $p < 0.01$), and ST2 (663.9 [387.8–772.5] vs. 190.5 [76.6–447.3] ng/mL; $p < 0.001$) (Figure 1B). By contrast, circulating KLF4 was significantly lower in TA-TMA plasma (43.8 [37.7–56.8] pg/mL) than in controls (56.5 [47.9–88.1] pg/mL; $p < 0.01$) (Figure 1C). Assessment of these markers in patients with aGVHD or active infection (Figure S1A–C) showed that the combination of elevated

C3b/sC5b-9 and reduced KLF4 is relatively specific to TA-TMA. Notably, a small proportion of TA-TMA cases also presented with concomitant aGVHD and/or infections, which may partially account for the overlapping biomarker ranges among cohorts.

Using flow cytometry to analyze circulating endothelial cells (CECs), we found that TA-TMA patients displayed significantly higher proportions of mature CECs (mCECs) (Figure S1D) and resting CECs (rCECs) (Figure S1E) compared with controls, whereas endothelial progenitor cells (EPCs) (Figure S1D) and activated CECs (aCECs) (Figure S1E) did not differ significantly. Further quantification indicated that, per 1 million peripheral blood mononuclear cells, TA-TMA patients had 88.5 ± 38.31 mCECs versus 22.5 ± 7.706 in controls ($p < 0.001$), and 92.5 ± 40.24 rCECs versus 24 ± 8.969 in controls ($p < 0.001$) (Table S2).

To mimic an in vivo TA-TMA milieu, we developed an indirect model in which HUVECs were incubated with TA-TMA plasma. After incubation, non-adherent cells were collected as CEC surrogates (termed “CECs” in figures), whereas firmly adherent cells represented intact endothelium (termed “HUVECs” in figures); both fractions were subjected to RNA-seq. In the resulting MA plot highlighting complement and endothelial function (Figure 1D), KLF4 exhibited relatively high baseline expression in HUVECs but was markedly downregulated in CECs. Consistent with the transcriptomic data, protein analyses ($p < 0.05$, Figure 1E) confirmed that KLF4 levels were indeed lower in CECs than in HUVECs. Taken together, these findings imply that diminished KLF4 expression

compromises the endothelial injury resistance.

Effects of KLF4 stimulation on complement deposition and endothelial injury induced by TA-TMA plasma.

To validate the in vitro model, we incubated HUVECs with plasma from controls, infection cases, aGVHD patients, and TA-TMA patients. Flow-cytometric analysis revealed a significant increase in surface C3 deposition exclusively in the TA-TMA group (Figure S2A), confirming both the robustness and specificity of the model for downstream experiments. Next, to assess KLF4's therapeutic potential, we pretreated HUVECs with the KLF4 stimulator APTO253 (MCE, #HY-16291) for 24h. Flow cytometry showed significant C3 (Figure S2B) and C5b-9 (Figure S2C) elevation in HUVECs incubated with TA-TMA plasma (termed "TMA plasma" in figures) versus control plasma ("Ctrl plasma" in figures). APTO253 (10 μM) partially reversed this effect. Hence, 10 μM was chosen for further in vitro experiments. Western blot confirmed KLF4 upregulation at this concentration (Figure S2D).

We next examined the expression of multiple complement components in HUVECs. Compared with control plasma, TA-TMA plasma significantly increased the mannose-binding lectin pathway component MBL2; the alternative pathway component CFB; C4, which converges the classical and mannose-binding lectin pathways; and the complement convergence points C3 and C5, but did not affect the classical pathway component C1QA. Treatment with APTO253 reduced these elevated complement

proteins (C3, C5, C4, CFB, and MBL2) (Figure S2E). Consistent with this, immunofluorescence staining revealed that deposition of activated complement components (C3, C5b-9, C5, C4, CFB, and MBL2) was heightened in HUVECs exposed to TA-TMA plasma but inhibited by APTO253 (Figure S2F).

We then evaluated the expression of proinflammatory and prothrombotic endothelial markers. TA-TMA plasma incubation elevated *ICAM-1* (Figure S2G), *VCAM-1* (Figure S2H), and *PAI-1* (Figure S2I), while decreasing *nitric oxide synthase 3* (*NOS3*) (Figure S2J) and *THBD* (Figure S2K). Notably, APTO253 restored these alterations, reducing *ICAM-1*, *VCAM-1*, and *PAI-1* and rescuing the expression of *NOS3* and *THBD*.

To confirm the protective role of KLF4, we constructed a KLF4 overexpression lentiviral vector (designated OEKLF4). Successful transduction was verified by flow cytometry (Figure S3A), and significantly higher *KLF4* mRNA and protein levels were confirmed (Figures S3B, C). Flow cytometry revealed that KLF4 overexpression markedly decreased C3 ($p < 0.0001$, Figure 2A) and C5b-9 deposition in OEKLF4 cells incubated with TA-TMA plasma compared with the vector control (designated PCDH) ($p < 0.0001$, Figure 2B). Western blot corroborated these findings, demonstrating reduced C3, C5, C4, CFB, and MBL2 proteins in OEKLF4 cells ($p < 0.05$, Figure 2C, Figure S3D-F), which was further validated by immunofluorescence (Figure S3G). In parallel, qPCR demonstrated that KLF4 overexpression lowered *ICAM-1*, *VCAM-1*, and *PAI-1* levels while enhancing *NOS3* and *THBD* under TA-TMA plasma challenge (Figure S3H-L).

Functionally, KLF4 overexpression mitigated plasma-induced disruptions of endothelial barrier integrity, as evidenced by preserved transendothelial electrical resistance ($p < 0.0001$, Figure 2D) and decreased fluorescein isothiocyanate-dextran leakage ($p < 0.0001$, Figure 2E) by established methods.[30] Flow cytometry confirmed reduced apoptosis in OEKLF4 versus the controls ($p < 0.0001$, Figure 2F).

KLF4 upregulates *CD46* expression in HUVECs

To clarify the mechanisms of KLF4-mediated endothelial protection, we performed CUT&Tag profiling with an anti-KLF4 antibody (Bio-Techne, #AF3640). This ultra-sensitive method provides base-pair-resolution maps of transcription-factor binding while maintaining minimal background noise. KLF4 overexpression reduced transcription start site (TSS) signals (Figures S4A, B) but increased promoter-region occupancy by 65.7% (Figure S4C), demonstrating its promoter-binding specificity. Further functional annotation of promoter-region peaks via Kyoto Encyclopedia of Genes and Genomes (KEGG) pathway analysis revealed significant enrichment in pathways tied to adherens junctions, tight junctions, leukocyte transendothelial migration, and apoptosis (Figure S4D), highlighting KLF4's broad regulatory influence on endothelial homeostasis.

Parallel RNA-seq of TA-TMA plasma-stimulated HUVECs revealed that KLF4 overexpression significantly altered gene expression compared to controls, with distinct upregulated and downregulated subsets. (Figure S4E). Consistent with the CUT&Tag

findings, KEGG enrichment of the upregulated genes indicated prominent involvement in the ECM–receptor interaction pathway (Figure S4F). By integrating the CUT&Tag peaks with these transcriptomic profiles, we identified 46 genes that not only displayed higher mRNA levels under KLF4 overexpression but also exhibited increased KLF4 occupancy at their promoter regions (Figure S4G).

Focusing on complement regulatory genes, we identified *CD46*, a complement-inhibiting membrane cofactor protein, as a direct KLF4 target. CUT&Tag signals showed markedly enhanced KLF4 binding at the *CD46* promoter after TA-TMA plasma stimulation (Figure 3A). Subsequent qPCR of immunoprecipitated genomic DNA confirmed enrichment of KLF4 at this locus (Figure 3B). Moreover, luciferase reporter assays demonstrated that KLF4 strongly induced *CD46* promoter activity (Figure 3C), and qPCR analysis revealed significantly increased *CD46* mRNA in KLF4-overexpressing HUVECs (Figure 3D). KLF4 selectively up-regulates *CD46* transcription in the TA-TMA milieu; by contrast, when HUVECs OEKLF4 were stimulated with aGVHD- or infection-derived plasma, *CD46* mRNA levels remained indistinguishable from those in PCDH controls (Figure S4H, I).

To pinpoint the promoter elements mediating KLF4-driven *CD46* transcription, we predicted KLF4-binding sites in the *CD46* promoter using Jaspar (Table S3) and performed in silico knockout by Basenji, disrupting three candidate sites (labeled 1, 2, and 3) (Figure 3E). Figure 3F shows ablating site 2 or 3 individually significantly decreased the predicted *CD46* expression score versus wild-type sequence, underscoring their roles in

CD46 transcriptional activity ($p<0.001$). Together, these results demonstrate that KLF4 directly regulates *CD46* to protect endothelium in TA-TMA.

To validate KLF4-mediated protection through CD46, we conducted phenotypic rescue experiments using stable CD46 knockdown HUVECs (designated ShCD46) (Figure S4J) treated with 10 μM APTO253. While APTO253 reduced C3 and C5b-9 deposition in control cells (designated PLKO.1), it failed to do so in ShCD46 cells (Figures 4A, B). Similarly, Western blot analysis revealed that APTO253 did not lower C3, C5, C4, CFB, or MBL2 in ShCD46 HUVECs exposed to TA-TMA plasma (Figure 4C, Figure S4K-M), nor did it reduce elevated *ICAM-1*, *VCAM-1*, or *PAI-1* mRNA levels (Figures 4D-F). Collectively, these findings indicate that the endothelial protection conferred by KLF4 largely depends on its upregulation of CD46.

Upregulation of KLF4 attenuates the TA-TMA phenotype in a mouse model

We next evaluated KLF4's protective effect in our DMOG-induced TA-TMA mouse model.[29] BALB/C mice post-allo-HSCT received APTO253 or vehicle (DMSO) per in Figure S5A, with Western blot confirming KLF4 upregulation ($p<0.01$, Figure S5B). APTO253-treated mice exhibited higher hemoglobin levels (192.0 ± 9.832 vs. 163.5 ± 3.900 g/L, $p<0.05$) (Figure S5C) and platelet counts (1273 ± 259.8 vs. 686.6 ± 214.4 × 10^9/L, $p<0.01$) (Figure S5C) than vehicle-treated mice, along with fewer schistocytes (Figure S5D). Additionally, APTO253 reduced serum lactate dehydrogenase (LDH) (1134 ± 176.3 vs. 4019 ± 1704 U/L, $p<0.001$) (Figure S5E), blood urea nitrogen (BUN) (20.58 ±

2.134 vs. 30.50 ± 4.604 mg/dL, p<0.001) (Figure S5F), and sC5b-9 (1211 ± 119.8 vs. 1556 ± 144.0 ng/mL, p<0.001) (Figure S5G) versus vehicle.

Histological analysis using hematoxylin and eosin (H&E) and periodic acid-Schiff (PAS) staining showed that APTO253 ameliorated TA-TMA–associated kidney lesions, including reduced glomerular capillary congestion, endothelial swelling, and detachment (Figure S5H). Immunofluorescence revealed decreased C3/C5b-9 deposition in APTO253-treated renal sections (Figure S5I). Since glomerular endothelial cell (GenC) injury is frequently associated with transcriptional changes in key endothelial genes, we measured the mRNA levels of *Icam-1*, *Vcam-1*, and *Pai-1*, all of which were elevated in DMOG-induced mice but were reduced upon APTO253 treatment (Figure S5J-L). APTO253 also partially restored *vascular endothelial growth factor-a* (*Vegfa*) mRNA (Figure S5M), whose deficiency is linked to TMA.[31] Corroborating these findings, plasma levels of ICAM-1 (78.97 ± 9.338 vs. 99.97 ± 14.06 ng/mL, p < 0.05) (Figure S5N), VCAM-1 (486.5 ± 70.80 vs. 744.6 ± 74.44 ng/mL, p < 0.0001) (Figure S5O), and PAI-1 (37.81 ± 5.231 vs. 57.38 ± 9.77 ng/mL, p < 0.001) (Figure S5P) were diminished after APTO253 administration. While survival rates trended higher with APTO253, the difference was not statistically significant (Figure S5Q).

To further validate the protective role of KLF4, we overexpressed it in vivo, following the protocol in Figure S6A. Ex vivo qPCR and Western blot analyses confirmed successful KLF4 overexpression in renal tissues (Figures S6B, C). Compared with vector-treated

mice, KLF4-overexpressing mice had significantly elevated hemoglobin levels (195.2 ± 9.538 vs. 159.0 ± 13.27 g/L, $p < 0.0001$) (Figure 5A) and platelet counts (1217 ± 132.3 vs. 915.8 ± 117.1×10^9/L, $p < 0.01$) (Figure 5A) and showed fewer schistocytes (Figure 5B). Serum levels of LDH (1238 ± 313.2 vs. 3722 ± 1486 U/L, $p < 0.01$) (Figure 5C), BUN (20.71 ± 2.228 vs. 33.68 ± 9.169 mg/dL, $p < 0.01$) (Figure S6D), and sC5b-9 (1141 ± 62.09 vs. 1544 ± 222.0 ng/mL, $p < 0.01$) (Figure S6E) were also reduced. Histologically, H&E and PAS staining revealed marked improvements in TA-TMA pathology, including diminished glomerular congestion and endothelial cell damage (Figure 5D), while Immunofluorescence showed decreased C3/C5b-9 deposition (Figure 5E).

Additionally, qPCR revealed that KLF4 overexpression markedly reduced *Icam-1*, *Vcam-1*, and *Pai-1* expression while increasing *Vegfa* levels compared with the vector group (Figure S6F-I). Plasma concentrations of ICAM-1 (79.35 ± 10.22 vs. 102.5 ± 14.61 ng/mL, $p < 0.05$) (Figure S6J), VCAM-1 (534.4 ± 105.8 vs. 767.9 ± 89.80 ng/mL, $p < 0.01$) (Figure S6K), and PAI-1 (37.96 ± 4.431 vs. 57.25 ± 13.78 ng/mL, $p < 0.01$) (Figure S6L) were also partially reversed in mice receiving mKLF4 plasmid. Notably, mKLF4 plasmid significantly improved survival versus vector controls (Figure 5F), highlighting its therapeutic potential in TA-TMA.

Statins ameliorate TA-TMA in a mouse model by upregulating KLF4 expression

Previous research indicates that endothelial KLF4 mediates statin-induced renoprotection in ischemic AKI by regulating cell adhesion molecules and inflammation.[27] Further studies

reveal that vasoprotective statins can robustly induce KLF2/KLF4 expression.[32, 33] Inspired by these findings, we evaluated statins in our TA-TMA mouse model. Pravastatin administration (Figure S7A) increased renal KLF4 ($p < 0.01$, Figure S7B).

Pravastatin-treated mice displayed significantly higher hemoglobin levels (206.8 ± 8.909 vs. 183.2 ± 5.134 g/L, $p < 0.01$) (Figure 6A) and platelet counts (1181 ± 165.1 vs. 875.0 ± 142.1 $\times 10^9$/L, $p < 0.05$) (Figure 6A), with a lower proportion of schistocytes than the vehicle group (Figure 6B). Serum LDH (1032 ± 320.5 vs. 3077 ± 1010 U/L, $p < 0.001$) (Figure 6C), BUN (22.40 ± 1.834 vs. 30.16 ± 8.513 mg/dL, $p < 0.05$) (Figure S7C), and sC5b-9 (1165 ± 121.7 vs. 1540 ± 276.6 ng/mL, $p < 0.01$) (Figure S7D) levels were notably reduced after pravastatin treatment. Histological assessment showed improved TA-TMA–related pathology in pravastatin-treated mice (Figure 6D). Immunofluorescence revealed substantially reduced renal deposits of C3 and C5b-9 (Figure 6E).

At the molecular level, pravastatin treatment also lowered the mRNA levels of *Icam-1*, *Vcam-1*, and *Pai-1*, while upregulating *Vegfa* compared with the vehicle group (Figure S7E-H). Correspondingly, plasma ICAM-1 (81.38 ± 8.394 vs. 100.5 ± 14.96 ng/mL, $p < 0.05$) (Figure S7I), VCAM-1 (458.3 ± 177.6 vs. 782.0 ± 191.1 ng/mL, $p < 0.01$) (Figure S7J), and PAI-1 (42.16 ± 2.785 vs. 64.43 ± 20.28 ng/mL, $p < 0.05$) (Figure S7K) concentrations were partially reversed in pravastatin-treated mice. Although these mice exhibited a higher overall survival rate than the vehicle group, the difference was not statistically significant (Figure 6F). Nonetheless, these results suggest pravastatin may

protect the endothelium in TA-TMA, possibly via KLF4.

Discussion

TA-TMA remains a life-threatening transplant complication, driven by complement dysregulation and endothelial dysfunction. However, many aspects—particularly how early endothelial injury contributes to disease onset—remain incompletely understood. Given the endothelium's function in vascular homeostasis, interventions preserving endothelial integrity could improve TA-TMA management.

In this study, we observed that plasma KLF4 levels tended to be lower concomitant with elevated C3b/sC5b-9 and endothelial injury markers in TA-TMA patients, although their distributions partially overlapped. Restoring KLF4 expression in vitro reduced complement deposition on HUVECs challenged with TA-TMA plasma, attenuated endothelial injury, and reinforced barrier function. Consistent with these findings, KLF4 overexpression in a murine TA-TMA model mitigated clinical and histological evidence of disease, indicating that KLF4 exerts protective effects on the endothelium.

TA-TMA pathophysiology originates from early endothelial damage, which triggers complement activation and microthrombus formation. We and others have observed elevated levels of ICAM-1, VCAM-1, PAI-1, and ST2 in TA-TMA patients, underscoring endothelial involvement.[19-21] Identifying the specific complement pathways (classical, lectin, or alternative) engaged in TA-TMA could reveal damage-associated molecular

patterns expressed by vulnerable tissues. In our in vitro model, we found that the lectin pathway appeared to be the initial trigger of complement-mediated damage, while the alternative pathway served as a key amplifier of endothelial injury. This partial divergence from other studies may reflect limitations of our model, as TA-TMA pathophysiology often involves either inherited or acquired defects in regulating both the classical and alternative pathways.[34]

KLF4 maintains endothelial homeostasis primarily by regulating anti-inflammatory and antithrombotic pathways.[23, 24] In TA-TMA patients, KLF4 downregulation coincided with elevated endothelial injury markers, implying its suppression exacerbates microvascular damage. This aligns with prior reports that KLF4 expression negatively correlates with prothrombotic genes, such as *PAI-1*, and positively correlates with *THBD* across TMA subtypes.[35, 36] Our finding that in vitro KLF4 upregulation mitigates TA-TMA-plasma-induced endothelial injury corroborates earlier reports that KLF4 boosts *NOS3* and *THBD* expression while down-regulating *VCAM-1* and pro-coagulant factors such as *tissue factor* and *PAI-1*.[23] Furthermore, in the TA-TMA microenvironment, KLF4 appears to safeguard endothelial barrier integrity chiefly by strengthening intercellular junctions and limiting cellular detachment, rather than by promoting cell migration as previously suggested.[37] Importantly, we provide the first evidence that KLF4's protective effect depends on *CD46* upregulation, as CD46 knockdown abolished KLF4-mediated rescue in HUVECs. These findings highlight a novel KLF4–CD46 axis central to complement regulation and endothelial protection in TA-TMA.

Beyond inhibiting cholesterol biosynthesis, statins exert pleiotropic endothelial-protective effects by enhancing endothelial nitric oxide synthase and thrombomodulin[38] while reducing leukocyte adhesion.[39] Endothelial KLF4 is essential for statin-mediated kidney protection in ischemic AKI, acting by regulating adhesion molecules and inflammation.[27] In line with these findings, we observed that pravastatin administration significantly improved the TA-TMA phenotype in our mouse model, suggesting that statin-induced KLF4 upregulation may protect the endothelium.

Mechanistically, KLF4 directly binds to the promoter of *CD46*, upregulating its transcription and thereby dampening complement activation, endothelial injury, and microthrombus formation. CD46-a cofactor for factor I-cleaves C3b and C4b, shielding endothelium from complement-mediated lysis.[40] Moreover, defects in factor H or CD46 underlie certain cases of non-infectious HUS,[41] and CD46 has been reported to protect the transplanted endothelium from recurrent HUS in the majority of affected patients.[42]

Notably, our findings point to an intricate link between KLF4's anti-inflammatory and antithrombotic roles and endothelial complement regulation.[43] For instance, KLF4 modulates *CD55* in intestinal epithelial cells,[25] while endothelial KLF4 deficiency increases TMA susceptibility through CD55 reduction.[44] Although previous studies focused mainly on C5b-9–mediated damage or factor H/I–mediated upstream regulation, we identify the KLF4–CD46 axis as a novel complement "brake"—supported by *CD46*

mutations found specifically in TA-TMA patients.[6] Collectively, these findings indicate that KLF4/CD46 likely collaborates with factor H, CD55, CD59, and other regulatory proteins to maintain endothelial homeostasis. Further studies should determine whether KLF4–CD46 interactions involve direct transcriptional control or multi-pathway mechanisms in TA-TMA endothelial protection.

Current TA-TMA management focuses on mitigating triggers through early supportive care, infection control, and calcineurin inhibitor withdrawal when possible. While available therapies have improved outcomes in high-risk cases, mortality rates still surpass 30%.[14, 15] Evidence from animal models suggests that broad measures to enhance endothelial health can protect against various TMAs,[45] highlighting the prophylactic value for HSCT complications like TA-TMA.

Our findings demonstrate that KLF4 exerts protective effects in DMOG-induced TA-TMA mice. Pravastatin administration not only ameliorated the disease phenotype but also upregulated KLF4 in renal tissues, suggesting that statins may confer endothelial protection partly by boosting KLF4 in susceptible organs like kidneys. However, KLF4 upregulation represents just one component of statins' pleiotropic effects. Further studies should explore KLF4's therapeutic potential in TA-TMA, including enhancing KLF4/CD46 in high-risk patients. Synergy with established protocols, such as co-administration of statins and complement inhibitors, could bolster therapeutic efficacy or permit dosage reduction. Nonetheless, safety assessments of KLF4 overexpression on hematopoiesis

and immunity require rigorous validation.

Limitations of our study include the potential systemic impact of KLF4 upregulation, even though mKLF4 plasmid delivery exhibits some organ specificity. Developing endothelial-specific *KLF4* transgenic or knockdown mouse models would help verify the tissue specificity of KLF4's protective effects and more precisely define its functional role. Moreover, we primarily investigated the KLF4–CD46 axis; additional studies are needed to examine KLF4's interactions with other complement, immunological, or coagulation pathways. Finally, despite our in vitro and in vivo models being validated for TA-TMA,[29, 46] they only partially capture the intricate pathophysiology of the disease, highlighting the need of KLF4 studies in alternative TA-TMA models.

In summary, our findings establish KLF4 as a pivotal regulator of endothelial homeostasis in TA-TMA by enhancing CD46 expression and suppressing pro-inflammatory, pro-thrombotic pathways (Figure 7). These results advocate for strategies that preserve or enhance KLF4 activity—whether through direct manipulation or via adjunctive agents such as statins—to mitigate the incidence and severity of TA-TMA. Further mechanistic and clinical studies are essential to optimize these approaches and alleviate TA-TMA's disease burden.

References

1. Jodele S, Davies SM, Lane A, et al. Diagnostic and risk criteria for HSCT-associated thrombotic microangiopathy: a study in children and young adults. Blood. 2014;124(4):645-653.

2. Schoettler ML, Carreras E, Cho B, et al. Harmonizing Definitions for Diagnostic Criteria and Prognostic Assessment of Transplantation-Associated Thrombotic Microangiopathy: A Report on Behalf of the European Society for Blood and Marrow Transplantation, American Society for Transplantation and Cellular Therapy, Asia-Pacific Blood and Marrow Transplantation Group, and Center for International Blood and Marrow Transplant Research. Transplant Cell Ther. 2023;29(3):151-163.

3. Laskin BL, Goebel J, Davies SM, Jodele S. Small vessels, big trouble in the kidneys and beyond: hematopoietic stem cell transplantation-associated thrombotic microangiopathy. Blood. 2011;118(6):1452-1462.

4. Young JA, Pallas CR, Knovich MA. Transplant-associated thrombotic microangiopathy: theoretical considerations and a practical approach to an unrefined diagnosis. Bone Marrow Transplant. 2021;56(8):1805-1817.

5. Jodele S, Licht C, Goebel J, et al. Abnormalities in the alternative pathway of complement in children with hematopoietic stem cell transplant-associated thrombotic microangiopathy. Blood. 2013;122(12):2003-2007.

6. Jodele S, Zhang K, Zou F, et al. The genetic fingerprint of susceptibility for transplant-associated thrombotic microangiopathy. Blood. 2016;127(8):989-996.

7. Rodrigues EM, Ardissino G, Pintarelli G, et al. Gene Abnormalities in Transplant Associated-Thrombotic Microangiopathy: Comparison between Recipient and Donor's DNA. Thromb Haemost. 2022;122(7):1247-1250.

8. Wehner J, Morrell CN, Reynolds T, Rodriguez ER, Baldwin WM 3rd. Antibody and complement in transplant vasculopathy. Circ Res. 2007;100(2):191-203.

9. Carroll MC, Isenman DE. Regulation of humoral immunity by complement. Immunity. 2012;37(2):199-207.

10. Jodele S, Fukuda T, Vinks A, et al. Eculizumab therapy in children with severe hematopoietic stem cell transplantation-associated thrombotic microangiopathy. Biol Blood Marrow Transplant. 2014;20(4):518-525.

11. Jodele S, Dandoy CE, Lane A, et al. Complement blockade for TA-TMA: lessons learned from a large pediatric cohort treated with eculizumab. Blood.

2020;135(13):1049-1057.

12. Castelli M, Micò MC, Grassi A, et al. Safety and efficacy of narsoplimab in pediatric and adult patients with transplant-associated thrombotic microangiopathy: a real-world experience. Bone Marrow Transplant. 2024;59(8):1161-1168.

13. Ardissino G, Capone V, Tedeschi S, Porcaro L, Cugno M. Complement System as a New Target for Hematopoietic Stem Cell Transplantation-Related Thrombotic Microangiopathy. Pharmaceuticals (Basel). 2022;15(7):845.

14. Rudoni J, Jan A, Hosing C, Aung F, Yeh J. Eculizumab for transplant-associated thrombotic microangiopathy in adult allogeneic stem cell transplant recipients. Eur J Haematol. 2018;101(3):389-398.

15. Bohl SR, Harsdorf S, Schoensteiner S, et al. Eculizumab Therapy of Adult TA-TMA: A High Response Rate Is Associated with a High Infection-Related Mortality. Blood. 2016;128(22):2255-2255.

16. Postalcioglu M, Kim HT, Obut F, et al. Impact of Thrombotic Microangiopathy on Renal Outcomes and Survival after Hematopoietic Stem Cell Transplantation. Biol Blood Marrow Transplant. 2018;24(11):2344-2353.

17. Schoettler M, Duncan C, Lehmann L. Severe, persistent neurotoxicity after transplant-associated thrombotic microangiopathy in a pediatric patient despite treatment with eculizumab. Pediatr Transplant. 2019;23(3):e13381.

18. Rajendran P, Rengarajan T, Thangavel J, et al. The vascular endothelium and human diseases. Int J Biol Sci. 2013;9(10):1057-1069.

19. Matsuda Y, Hara J, Osugi Y, et al. Serum levels of soluble adhesion molecules in stem cell transplantation-related complications. Bone Marrow Transplant. 2001;27(9):977-982.

20. Rotz SJ, Dandoy CE, Davies SM. ST2 and Endothelial Injury as a Link between GVHD and Microangiopathy. N Engl J Med. 2017;376(12):1189-1190.

21. Nurnberger W, Michelmann I, Burdach S, Gobel U. Endothelial dysfunction after bone marrow transplantation: increase of soluble thrombomodulin and PAI-1 in patients with multiple transplant-related complications. Ann Hematol. 1998;76(2):61-65.

22. Dvorak CC, Higham C, Shimano KA. Transplant-Associated Thrombotic Microangiopathy in Pediatric Hematopoietic Cell Transplant Recipients: A Practical Approach to Diagnosis and Management. Front Pediatr. 2019;7:133.

23. Hamik A, Lin Z, Kumar A, et al. Kruppel-like factor 4 regulates endothelial inflammation. J Biol Chem. 2007;282(18):13769-13779.

24. Zhou G, Hamik A, Nayak L, et al. Endothelial Kruppel-like factor 4 protects against atherothrombosis in mice. J Clin Invest. 2012;122(12):4727-4731.

25. Shao J, Yang VW, Sheng H. Prostaglandin E2 and Kruppel-like transcription factors synergistically induce the expression of decay-accelerating factor in intestinal epithelial cells. Immunology. 2008;125(3):397-407.

26. Villarreal GJr., Zhang Y, Larman HB, Gracia-Sancho J, Koo A, García-Cardeña G. Defining the regulation of KLF4 expression and its downstream transcriptional targets in vascular endothelial cells. Biochem Biophys Res Commun. 2010;391(1):984-989.

27. Yoshida T, Yamashita M, Iwai M, Hayashi M. Endothelial Kruppel-Like Factor 4 Mediates the Protective Effect of Statins against Ischemic AKI. J Am Soc Nephrol. 2016;27(5):1379-1388.

28. Qi J, Wang J, Chen J, et al. Plasma levels of complement activation fragments C3b and sC5b-9 significantly increased in patients with thrombotic microangiopathy after allogeneic stem cell transplantation. Ann Hematol. 2017;96(11):1849-1855.

29. Qi J, Pan T, You T, et al. Upregulation of HIF-1alpha contributes to complement activation in transplantation-associated thrombotic microangiopathy. Br J Haematol. 2022;199(4):603-615.

30. León J, Acurio J, Bergman L, et al. Disruption of the Blood-Brain Barrier by Extracellular Vesicles From Preeclampsia Plasma and Hypoxic Placentae: Attenuation by Magnesium Sulfate. Hypertension. 2021;78(5):1423-1433.

31. Eremina V, Jefferson JA, Kowalewska J, et al. VEGF inhibition and renal thrombotic microangiopathy. N Engl J Med. 2008;358(11):1129-1136.

32. Ohnesorge N, Viemann D, Schmidt N, et al. Erk5 activation elicits a vasoprotective endothelial phenotype via induction of Kruppel-like factor 4 (KLF4). J Biol Chem. 2010;285(34):26199-26210.

33. Komaravolu RK, Adam C, Moonen JR, Harmsen MC, Goebeler M, Schmidt M. Erk5 inhibits endothelial migration via KLF2-dependent down-regulation of PAK1. Cardiovasc Res. 2015;105(1):86-95.

34. Jodele S. Complement in Pathophysiology and Treatment of Transplant-Associated Thrombotic Microangiopathies. Semin Hematol. 2018;55(3):159-166.

35. Modde F, Agustian PA, Wittig J, et al. Comprehensive analysis of glomerular mRNA expression of pro- and antithrombotic genes in atypical haemolytic-uremic syndrome (aHUS). Virchows Arch. 2013;462(4):455-464.

36. Agustian PA, Bockmeyer CL, Modde F, et al. Glomerular mRNA expression of prothrombotic and antithrombotic factors in renal transplants with thrombotic microangiopathy. Transplantation. 2013;95(10):1242-1248.

37. Shan F, Huang Z, Xiong R, Huang QY, Li J. HIF1α-induced upregulation of KLF4 promotes migration of human vascular smooth muscle cells under hypoxia. J Cell Physiol. 2020;235(1):141-150.

38. Sen-Banerjee S, Mir S, Lin Z, et al. Kruppel-like factor 2 as a novel mediator of statin effects in endothelial cells. Circulation. 2005;112(5):720-726.

39. Eccles KA, Sowden H, Porter KE, Parkin SM, Homer-Vanniasinkam S, Graham AM. Simvastatin alters human endothelial cell adhesion molecule expression and inhibits leukocyte adhesion under flow. Atherosclerosis. 2008;200(1):69-79.

40. Liszewski MK, Post TW, Atkinson JP. Membrane cofactor protein (MCP or CD46): newest member of the regulators of complement activation gene cluster. Annu Rev Immunol. 1991;9:431-455.

41. Goodship TH, Liszewski MK, Kemp EJ, Richards A, Atkinson JP. Mutations in CD46, a complement regulatory protein, predispose to atypical HUS. Trends Mol Med. 2004;10(5):226-231.

42. Bresin E, Daina E, Noris M, et al. Outcome of renal transplantation in patients with non-Shiga toxin-associated hemolytic uremic syndrome: prognostic significance of genetic background. Clin J Am Soc Nephrol. 2006;1(1):88-99.

43. Jackson SP, Darbousset R, Schoenwaelder SM. Thromboinflammation: challenges of therapeutically targeting coagulation and other host defense mechanisms. Blood. 2019;133(9):906-918.

44. Estrada CC, Cardona S, Guo Y, et al. Endothelial-specific loss of Kruppel-Like Factor 4 triggers complement-mediated endothelial injury. Kidney Int. 2022;102(1):58-77.

45. Goldberg RJ, Nakagawa T, Johnson RJ, Thurman JM. The role of endothelial cell injury in thrombotic microangiopathy. Am J Kidney Dis. 2010;56(6):1168-1174.

46. Zhang R, Qi J, Zhou M, et al. Upregulation of Nrf2 Attenuates Oxidative Stress-Induced, Complement Activation-Associated Endothelial Injury and Apoptosis in Transplant-Associated Thrombotic Microangiopathy. Transplant Cell Ther. 2021;27(9):758.e1-758.e8.

Table1 Baseline and procedure characteristics before and after propensity score matching

	Before matching			After matching		
Variables	Control (n = 2367)	TA-TMA (n = 20)	p-value	Control (n = 20)	TA-TMA (n = 20)	p-value
Age, median (IQR)	39 (29, 51)	46 (30.25, 59.75)	0.064	48 (30.25, 54.25)	46 (30.25, 59.75)	0.495
Sex, n (%)			0.303			
Female	1039 (44)	11 (55)		8 (40)	11 (55)	0.342
Male	1348 (56)	9 (45)		12 (60)	9 (45)	
Diagnosis, n (%)			0.281			0.165
ALL	557 (23)	4 (20)		6 (30)	4 (20)	
AML	1132 (48)	9 (45)		9 (45)	9 (45)	
CML	40 (2)	0 (0)		1 (5)	0 (0)	
HAL	41 (2)	0 (0)		0 (0)	0 (0)	
MPAL	1 (0)	1 (5)		0 (0)	1 (5)	
MDS	367 (15)	4 (20)		0 (0)	4 (20)	
NHL	51 (2)	1 (5)		2 (10)	1 (5)	
SAA	169 (7)	1 (5)		1 (5)	1 (5)	
PNH	29 (1)	0 (0)		1 (5)	0 (0)	
HLA, n (%)			0.839			0.723
HLA-matched	645 (27)	5 (25)		6 (30)	5 (25)	
HLA-unmatched	1742 (73)	15 (75)		14 (70)	15 (75)	
Transplant source, n (%)			0.737			0.034
BM	20 (1)	0 (0)		0 (0)	0 (0)	
PB	2038 (85)	18 (90)		11 (55)	18 (90)	
BM + PB	329 (14)	2 (10)		9 (45)	2 (10)	

Donor recipient blood type, n (%)			0.457		0.891
Major unmatched	431 (18)	3 (15)	2 (10)	3 (15)	
Major + minor unmatched	178 (8)	3 (15)	2 (10)	3 (15)	
Matched	1269 (53)	8 (40)	10 (50)	8 (40)	
Minor unmatched	509 (21)	6 (30)	6 (30)	6 (30)	

Abbreviations: ALL, acute lymphoblastic leukemia; AML, acute myeloblastic leukemia; CML, chronic myelocytic leukemia; HAL, hybrid acute leukemia; MPAL, mixed phenotype acute leukemia; MDS, myelodysplastic syndromes; NHL, non-Hodgkin’ s lymphoma; SAA, severe aplastic anemia; PNH, paroxysmal nocturnal hemoglobinuria; HLA, human leucocyte antigen; BM, bone marrow; PB, peripheral blood; IQR, interquartile range.

Figure legends

Figure 1 | Transplant-associated thrombotic microangiopathy (TA-TMA) patients exhibit abnormal complement activation and endothelial injury.

A, Plasma levels of C3b (left panel), sC5b-9 (center panel), and intercellular cell adhesion molecule-1 (right panel) in TA-TMA patients and controls. n = 20 per group.

B, In the left, center, and right panels: Plasma levels of vascular cell adhesion molecule-1, plasminogen activator inhibitor-1, and suppression of tumorigenicity 2, respectively, in TA-TMA patients and controls. n = 20 per group.

C, Plasma levels of krüppel-like factor 4 (KLF4) in TA-TMA patients versus controls. n = 20 per group.

D, MA plot of complement/endothelium-associated differentially expressed genes (red: up-regulated; blue: down-regulated; grey: not significant; dashed horizontal lines: p-value thresholds) in HUVECs and circulating endothelial cells (CECs) from RNA sequencing analysis. n = 3 per group.

E, Western blot analysis of KLF4 protein levels in HUVECs and CECs. Bar graph shows the relative intensity of KLF4. The results are representatives of three experiments. n = 4 per group. *p < 0.05, **p < 0.01, ***p < 0.001, ****p < 0.0001.

Figure 2 | KLF4 overexpression reduces complement deposition and endothelial injury under TA-TMA plasma challenge.

A, B, Flow cytometric detection of C3 (A) and C5b-9 (B) in KLF4-overexpressing HUVECs (OEKLF4) and control lentiviral-transduced cells (PCDH) incubated with control or

TA-TMA plasma. Bar graphs show mean fluorescence intensities.

C, Western blot of complement proteins (C3, C5, C4, CFB, MBL2, C1QA) in these cells. Bar graphs compare the relative intensities of C3, C5 and C4.

D, Relative decrease (ΔTEER) of transendothelial electrical resistance in the indicated groups.

E, Fluorescein isothiocyanate-dextran permeability assay reflecting endothelial barrier integrity.

F, Flow cytometric analysis of apoptosis in PCDH and OEKLF4 cells treated with control or TA-TMA plasma. Bar graph shows the quantification of apoptotic cells.

The results are representatives of three experiments. *p < 0.05, ***p < 0.001, ****p < 0.0001.

Figure 3 | KLF4 transcriptionally activates *CD46* gene expression in HUVECs.

A, Integrative Genomics Viewer tracks of CUT&Tag showing enriched KLF4 in the promoter of *CD46*.

B, quantitative real-time PCR (qPCR) of genomic DNA isolated by CUT&Tag, confirming KLF4 enrichment at the *CD46* promoter.

C, Interaction between *CD46* promoter and KLF4 by Dural luciferase reporter assays. The results are representatives of three experiments.

D, *CD46* mRNA levels measured by qPCR in KLF4-overexpression (OEKLF4) and control lentiviral-transduced cells (PCDH) exposed to TA-TMA plasma. The results are representatives of three experiments.

E, Jaspar-based prediction of three KLF4-bingding sites in the *CD46* promoter identifies transcriptional regulatory elements.

F, Basenji in silico knockout identifies sites 2 and 3 as critical regulators of *CD46* transcriptional activity.

**p < 0.01, ***p < 0.001, ****p < 0.0001.

Figure 4 | KLF4-mediated protection is abrogated by CD46 knockdown.

A, B, Flow cytometric measurement of C3 (A) and C5b-9 (B) deposition in CD46 knockdown HUVECs (ShCD46) or control cells (PLKO.1) treated with control plasma, TA-TMA plasma, or TA-TMA plasma plus APTO253. Bar graphs show mean fluorescence intensities.

C, Western blot showing complement proteins (C3, C5, C4, CFB, MBL2) in each group. The bar graphs indicate the relative intensities of C3 and C5.

D–F, qPCR analysis of *ICAM-1* (D), *VCAM-1* (E), and *PAI-1* (F).

The results are representatives of three experiments. *p < 0.05, **p < 0.01, ***p < 0.001, ****p < 0.0001. ns, not significant.

Figure 5 | In vivo KLF4 overexpression attenuates TA-TMA pathology.

A, Hemoglobin (HGB) levels and platelet counts in mKLF4-transfected mice versus vector controls.

B, Representative peripheral blood smears (×100) illustrating fewer schistocytes (arrows) in KLF4-overexpressing mice. Scale bars: 10 μm.

C, Plasma lactate dehydrogenase (LDH) in the indicated groups.

D, Representative hematoxylin & eosin (H&E) and periodic acid–Schiff (PAS) staining showing glomerular structural improvement in mKLF4-transfected mice versus vector controls. Scale bar: 10 μm. Pound sign (#) indicates glomerular congestion; asterisk (★) indicates endothelial swelling/detachment.

E, Immunofluorescent detection of C3 and C5b-9 in renal tissue with Hoechst counterstain. The bar graphs show mean fluorescence intensities. Scale bars: 10 μm.

L, Kaplan–Meier survival curves showing significantly improved survival in KLF4-overexpressing mice.

The results are representatives of three experiments and six mice/group. *$p < 0.05$, **$p < 0.01$, ***$p < 0.001$, ****$p < 0.0001$. ns, not significant.

Figure 6 | Statin treatment ameliorates TA-TMA by upregulating KLF4.

A, HGB and platelet counts in mice treated with pravastatin or vehicle.

B, Peripheral blood smears (×100) showing fewer schistocytes (arrows) in pravastatin-treated mice. Scale bars: 10 μm.

C, Plasma LDH in each group.

D, Representative H&E and PAS staining of renal tissue demonstrating restored glomerular histology in mice treated with pravastatin (scale bar, 10 μm). Pound sign (#) indicates glomerular congestion; asterisk (★) indicates endothelial swelling/detachment.

E, Immunofluorescent staining of C3 and C5b-9 with Hoechst counterstain. The bar graphs show mean fluorescence intensities. Scale bars: 10 μm.

F, Kaplan–Meier survival curves for mice receiving pravastatin versus vehicle.

The results are representatives of three experiments and six mice/group. *p < 0.05, **p < 0.01, ***p < 0.001, ****p < 0.0001; ns, not significant.

Figure 7 | Schematic illustration.

Schematic diagram of KLF4 as a key negative regulator of complement-mediated endothelial injury in TA-TMA.

Figure 1

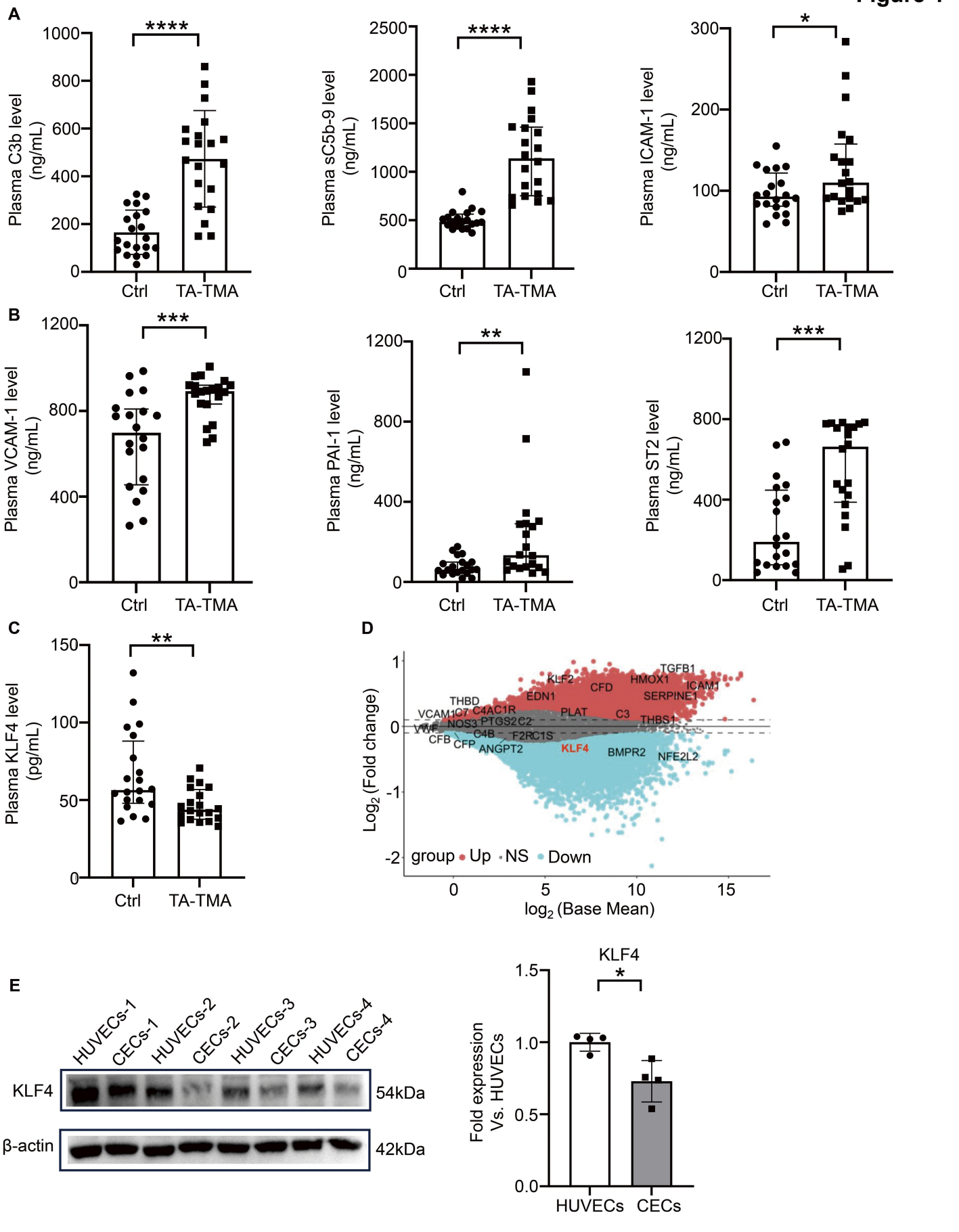
A
Plasma C3b level (ng/mL)
Plasma sC5b-9 level (ng/mL)
Plasma ICAM-1 level (ng/mL)
Ctrl
TA-TMA
B
Plasma VCAM-1 level (ng/mL)
Plasma PAI-1 level (ng/mL)
Plasma ST2 level (ng/mL)
C
Plasma KLF4 level (pg/mL)
D
Log2 (Fold change)
log2 (Base Mean)
group Up NS Down
KLF2
CFD
HMOX1
TGFB1
ICAM1
SERPINE1
EDN1
THBD
VCAM1
C7
C4AC1R
PLAT
C3
THBS1
NOS3
PTGS2
C2
VWF
C4B
F2RC1S
CFB
CFP
ANGPT2
KLF4
BMPR2
NFE2L2
E
HUVECs-1
CECs-1
HUVECs-2
CECs-2
HUVECs-3
CECs-3
HUVECs-4
CECs-4
KLF4
54kDa
β-actin
42kDa
KLF4
Fold expression Vs. HUVECs
HUVECs
CECs

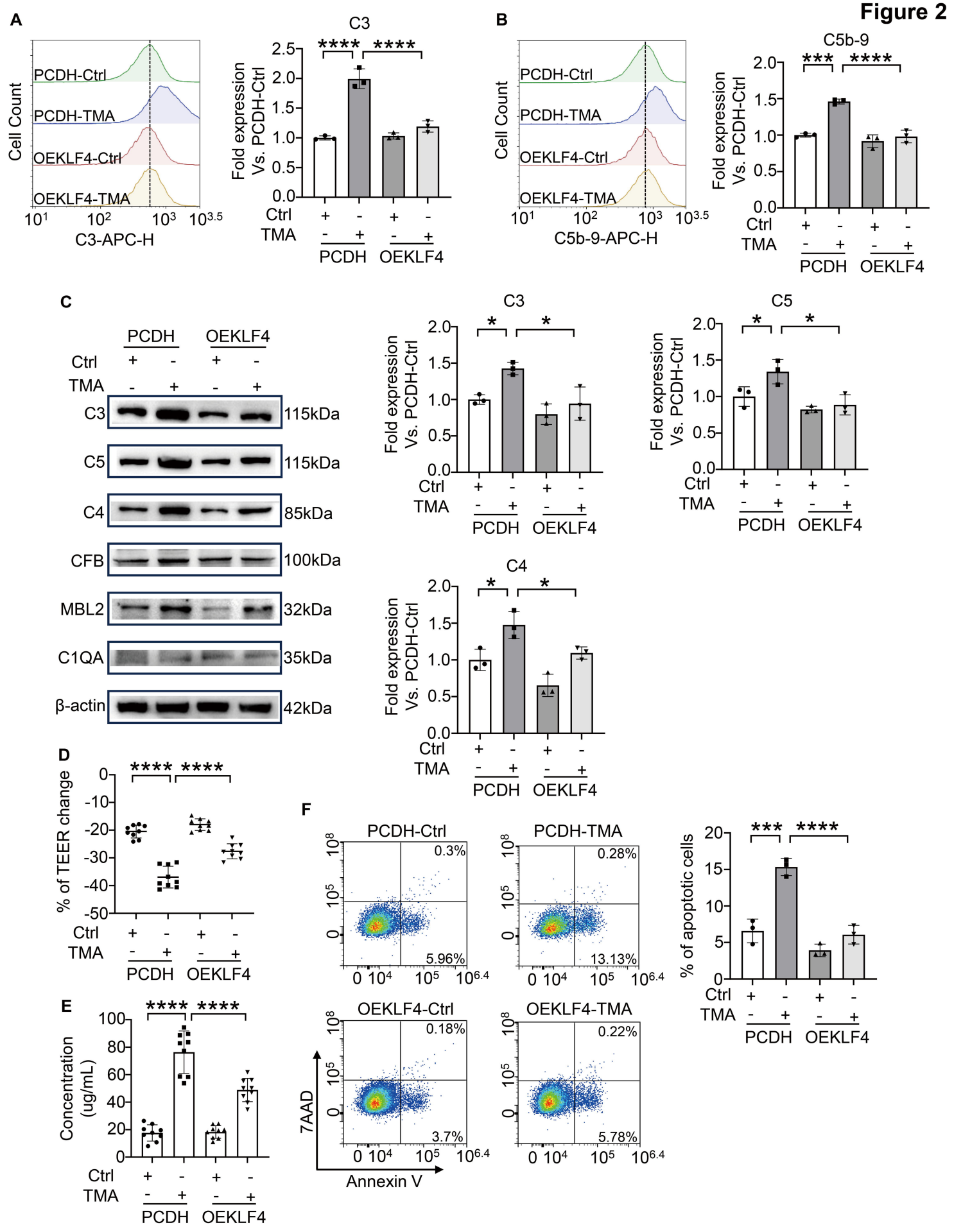
A
PCDH-Ctrl
PCDH-TMA
OEKLF4-Ctrl
OEKLF4-TMA
Cell Count
C3-APC-H
C3
Fold expression Vs. PCDH-Ctrl
Ctrl
TMA
PCDH
OEKLF4
B
C5b-9-APC-H
C5b-9
C
C3
C5
C4
CFB
MBL2
C1QA
β-actin
115kDa
85kDa
100kDa
32kDa
35kDa
42kDa
D
% of TEER change
E
Concentration (ug/mL)
F
0.3%
5.96%
0.28%
13.13%
0.18%
3.7%
0.22%
5.78%
7AAD
Annexin V
% of apoptotic cells

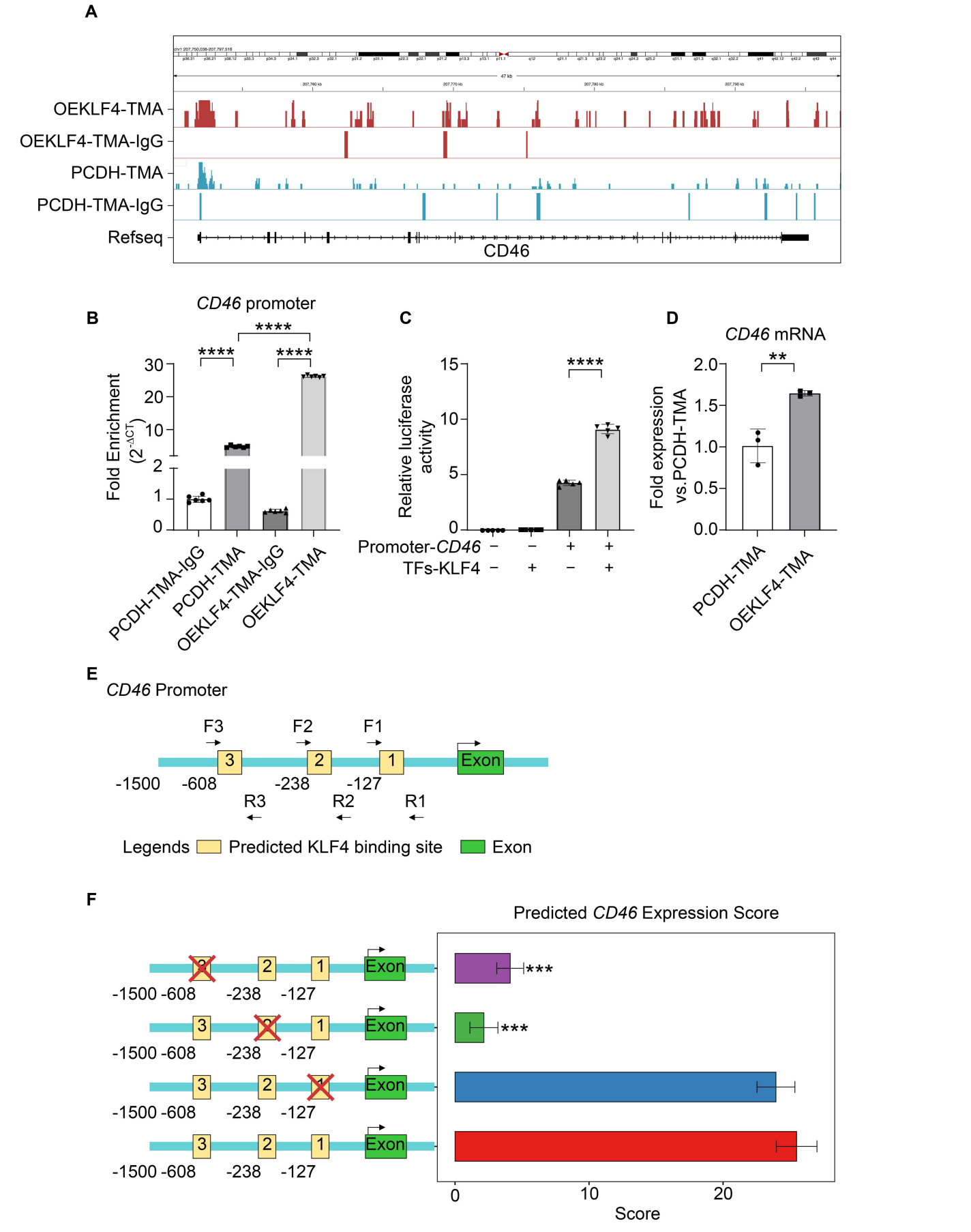
A
OEKLF4-TMA
OEKLF4-TMA-IgG
PCDH-TMA
PCDH-TMA-IgG
Refseq
CD46
B
CD46 promoter
Fold Enrichment (2^-ΔCT)
****
****
****
PCDH-TMA-IgG
PCDH-TMA
OEKLF4-TMA-IgG
OEKLF4-TMA
C
Relative luciferase activity
****
Promoter-CD46
TFs-KLF4
D
CD46 mRNA
Fold expression vs.PCDH-TMA
**
PCDH-TMA
OEKLF4-TMA
E
CD46 Promoter
F3
F2
F1
R3
R2
R1
Exon
-1500
-608
-238
-127
Legends
Predicted KLF4 binding site
Exon
F
Predicted CD46 Expression Score
***
***
Score

Figure 4

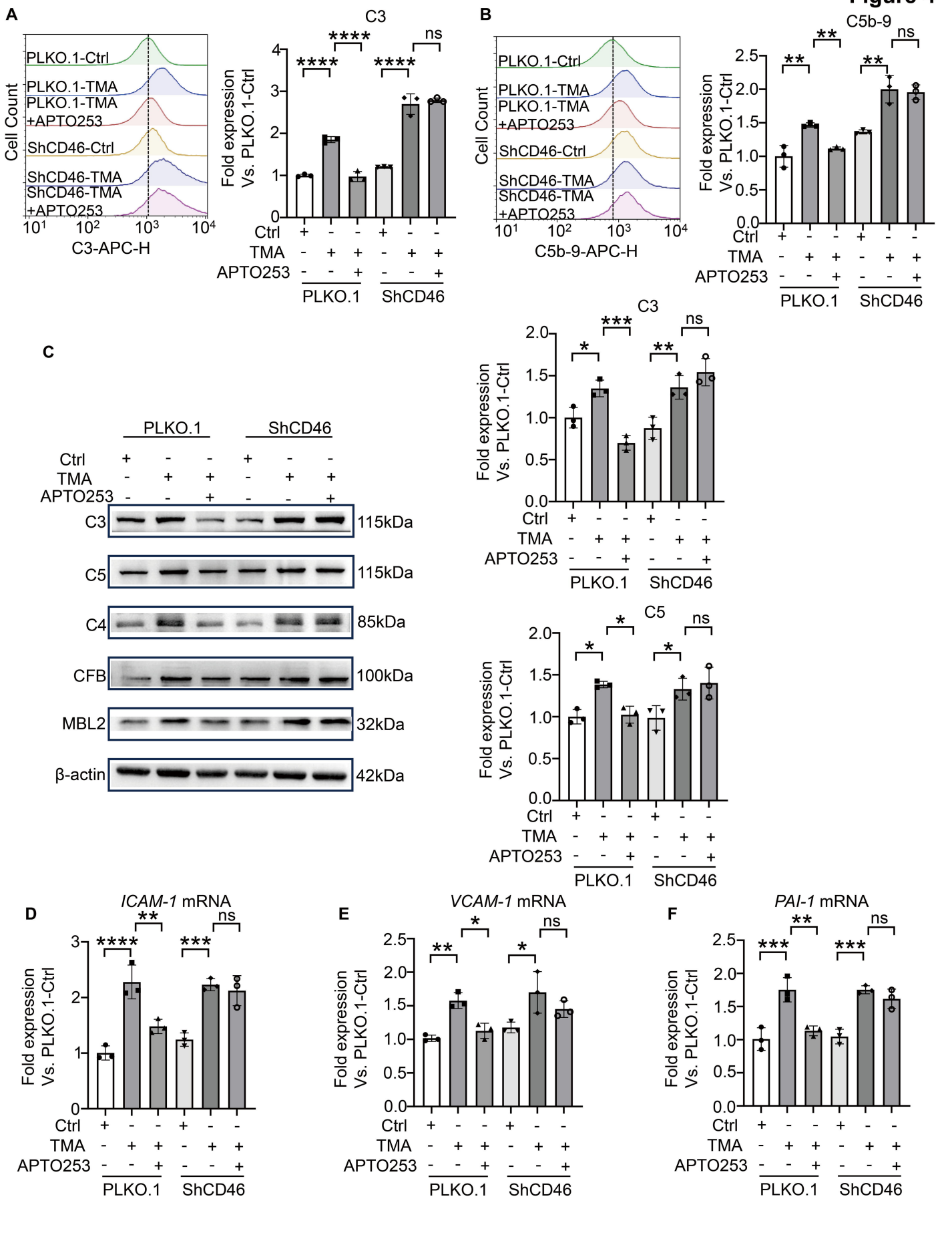
A
PLKO.1-Ctrl
PLKO.1-TMA
PLKO.1-TMA +APTO253
ShCD46-Ctrl
ShCD46-TMA
ShCD46-TMA +APTO253
Cell Count
C3-APC-H
C3
Fold expression Vs. PLKO.1-Ctrl
Ctrl
TMA
APTO253
PLKO.1
ShCD46
B
C5b-9-APC-H
C5b-9
C
PLKO.1
ShCD46
C3
C5
C4
CFB
MBL2
β-actin
115kDa
115kDa
85kDa
100kDa
32kDa
42kDa
C5
D
ICAM-1 mRNA
E
VCAM-1 mRNA
F
PAI-1 mRNA

Figure 5

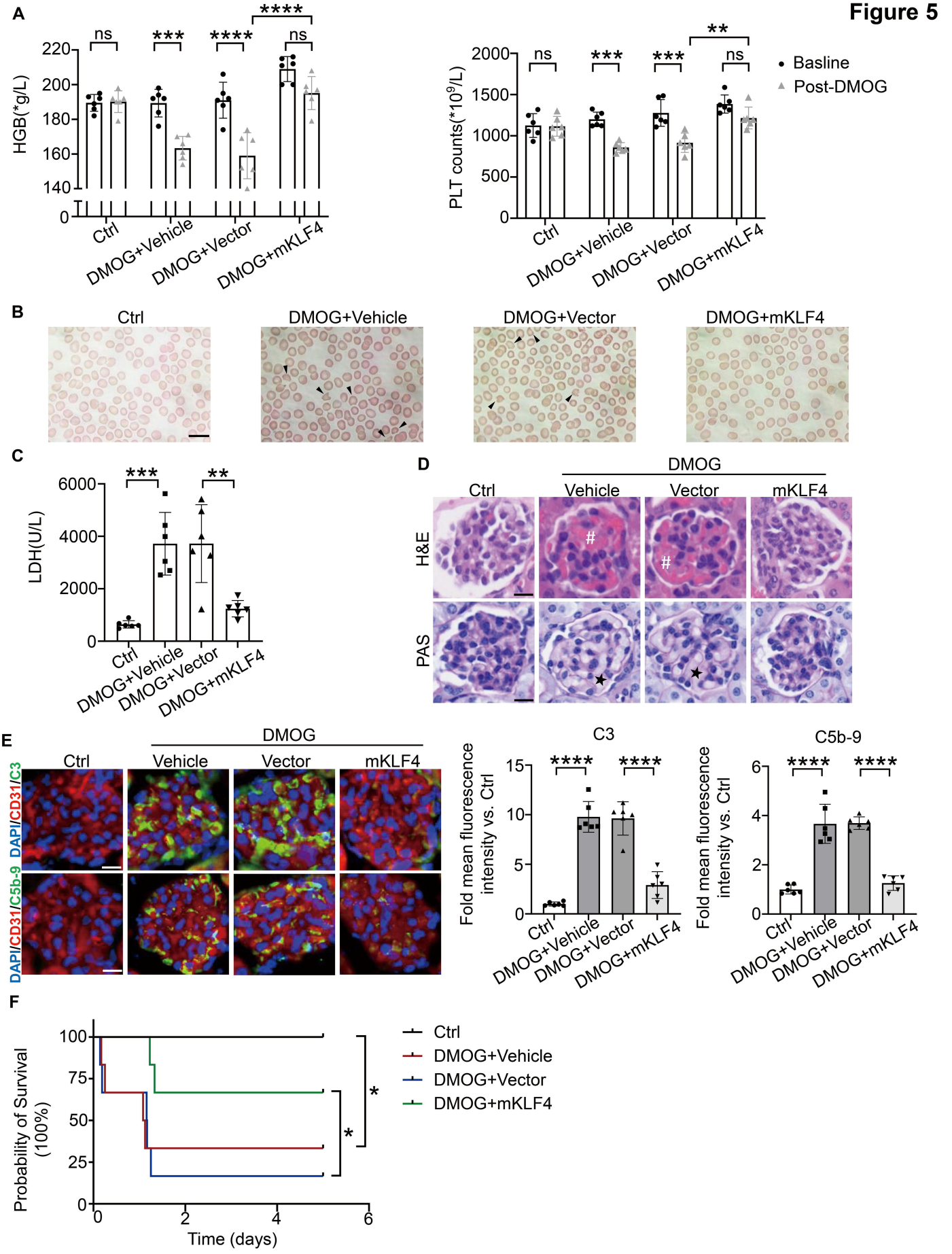
A
HGB(*g/L)
ns
***
****
ns
Ctrl
DMOG+Vehicle
DMOG+Vector
DMOG+mKLF4
PLT counts(*10^9/L)
**
Basline
Post-DMOG
B
Ctrl
DMOG+Vehicle
DMOG+Vector
DMOG+mKLF4
C
LDH(U/L)
D
DMOG
Ctrl
Vehicle
Vector
mKLF4
H&E
PAS
E
DAPI/CD31/C3
DAPI/CD31/C5b-9
C3
C5b-9
Fold mean fluorescence intensity vs. Ctrl
F
Probability of Survival (100%)
Time (days)

Figure 6

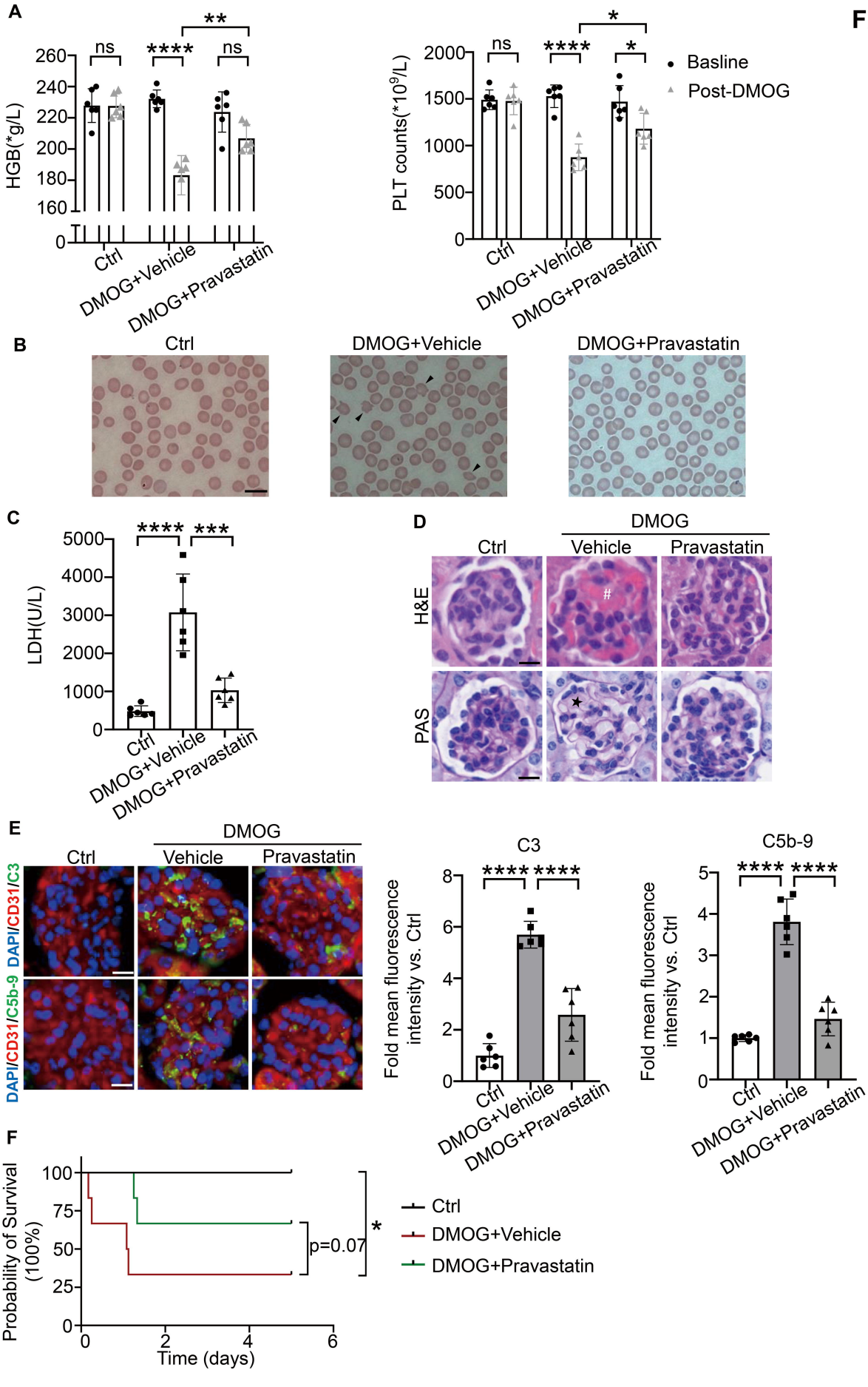
A
HGB(*g/L)
ns
****
ns
**
Ctrl
DMOG+Vehicle
DMOG+Pravastatin
PLT counts(*10^9/L)
Basline
Post-DMOG
B
Ctrl
DMOG+Vehicle
DMOG+Pravastatin
C
LDH(U/L)
D
DMOG
H&E
PAS
E
DAPI/CD31/C3
DAPI/CD31/C5b-9
C3
C5b-9
Fold mean fluorescence intensity vs. Ctrl
F
Probability of Survival (100%)
Time (days)
p=0.07

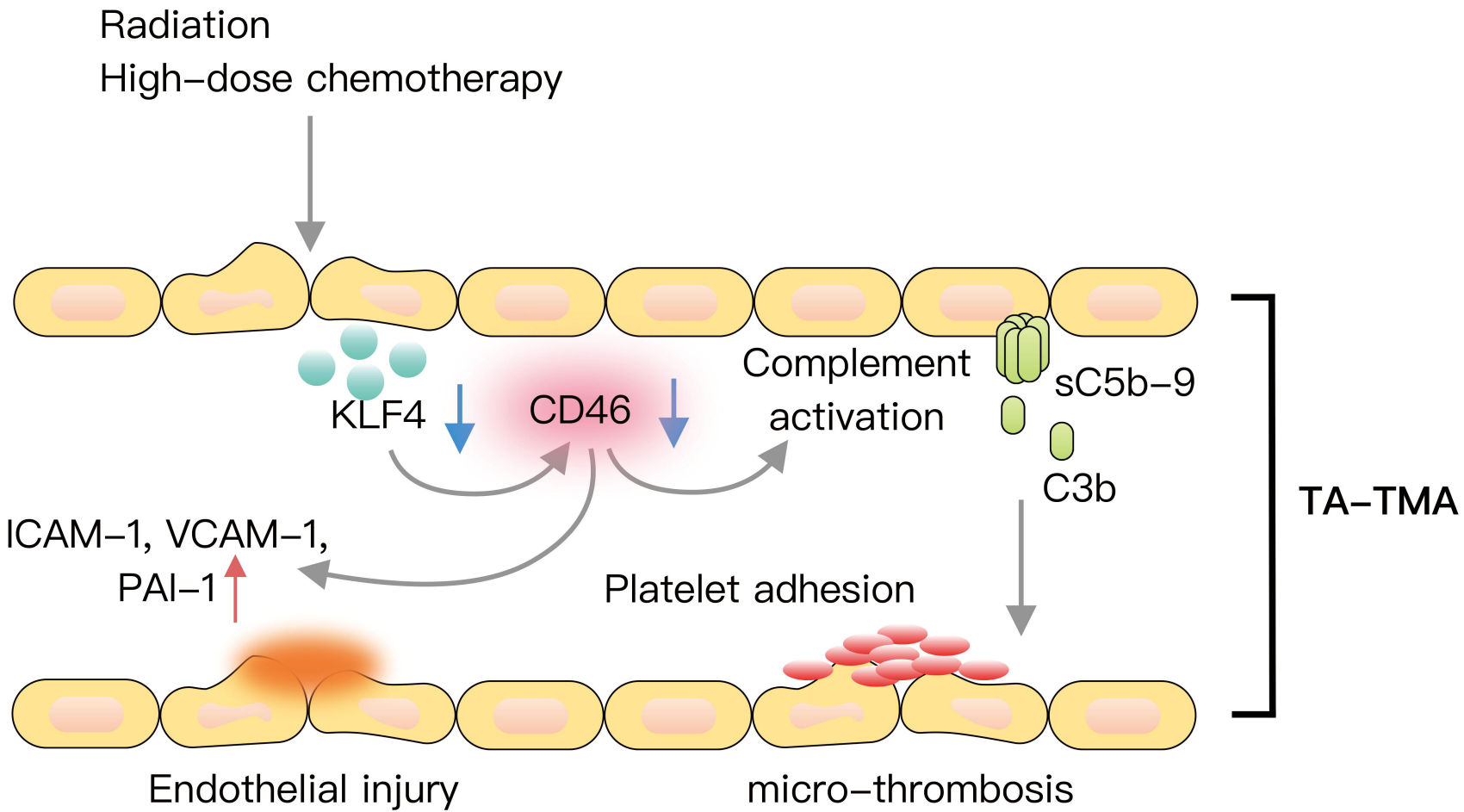
Radiation
High-dose chemotherapy
KLF4
CD46
Complement
activation
sC5b-9
C3b
TA-TMA
ICAM-1, VCAM-1,
PAI-1
Platelet adhesion
Endothelial injury
micro-thrombosis

Supplementary material

Supplementary methods

Definition of TA-TMA

According to the published diagnostic criteria proposed in 2023,[1] TA-TMA is diagnosed when at least four of the following seven features are documented on two occasions within a 14-day window:

1. **Anemia**—failure to attain transfusion independence after neutrophil engraftment, a ≥ 1 g/dL drop in hemoglobin, or new transfusion dependence.
2. **Thrombocytopenia**—failure to achieve platelet engraftment, higher-than-expected platelet transfusion requirements, refractoriness to platelet transfusion, or a ≥ 50% decline in baseline platelet count after full engraftment.
3. **Elevated lactate dehydrogenase (LDH)**—serum LDH above the upper limit of normal (ULN).
4. **Schistocytosis**—presence of schistocytes on blood smear.
5. **Hypertension**—new-onset or worsening hypertension.
6. **Elevated soluble C5b-9**—levels exceeding the ULN.
7. **Proteinuria**—random urine protein-to-creatinine ratio (rUPCR) ≥ 1 mg/mg.

Enzyme-linked immunosorbent assay

Human plasma levels of complement components (C3b and sC5b-9) (Novus, #NBP2-60553, CV% < 9.9%, detect range [0.156–5] ng/mL; Novus, #NBP2-66708, CV% < 5.07%, detect range [31.25–2000] ng/mL), inflammatory/thrombotic endothelial factors (ICAM-1,

VCAM-1, ST2, and PAI-1) (Cusbio, #CSB-E04574h, CV% < 10%, detect range [0.78–50] ng/mL; Cusbio, #CSB-E04753h, CV% < 10%, detect range [1.563–100] ng/mL; Cusbio, #CSB-E13789h, CV% < 10%, detect range [0.312–20] ng/mL; Proteintech, #KE00109, CV% < 2.6%, detect range [0.313–20] ng/mL) and KLF4 (Cusbio, #CSB-EL012394HU, CV% < 10%, detect range [18.75–1200] pg/mL) were measured using commercial enzyme-linked immunosorbent assay (ELISA) kits according to the manufacturers' instructions. Additionally, mouse plasma levels of sC5b-9 (Krishgen, #KLM0637, CV% < 10%, detect range [1.562–100] ng/mL), ICAM-1 (Proteintech, #KE10063, CV% < 2.7%, detect range [15.6–1000] pg/mL), VCAM-1 (Cusbio, #CSB-E04754m, CV% < 10%, detect range [39.062–2500] pg/mL) and PAI-1 (Cusbio, #CSB-E07947m, CV% < 10%, detect range [0.9–60] ng/mL) were assessed via ELISA.

Cell culture and treatment

Human umbilical vein endothelial cells (HUVECs; ATCC) were used to establish the complement-adherent in-vitro model as previously described.[2] To stimulate KLF4, cells were pre-treated with the small-molecule activator APTO-253 (MCE, #HY-16291) at 10 μM for 24 h before evaluating complement deposition and endothelial-injury markers.

To generate HUVEC cell lines with either KLF4 overexpression or CD46 knockdown, a lentiviral-mediated approach was employed. A lentiviral vector (pCDH-SFFV-IRES-EGFP) encoding full-length human KLF4 (designated OEKLF4) and its control lentiviral vector (designated PCDH) were purchased from General Biol Ltd. Additionally, a pLKO.1-CMV-

copGFP-PURO vector for CD46 knockdown (designated ShCD46) and its corresponding control vector (designated PLKO.1) were obtained from Beijing Tsingke Biotech Ltd.

Flow cytometry

A five-color flow cytometric assay[3] (phycoerythrin [PE]-conjugated anti-CD45, BioLegend, #982322; PE-cyanine [Cy7]–conjugated anti-CD34, BioLegend, #343515; allophycocyanin [APC]-Cy7–conjugated anti-CD146, BioLegend, #361041; APC-conjugated anti-CD133, BioLegend, #372805; brilliant violet-421–conjugated anti-CD106, BioLegend, #305815) was employed to detect and characterize CECs and their subpopulations in patients' peripheral blood. mCECs were defined as $CD34^+/CD45^-/CD133^-/CD146^+$; EPCs were identified as $CD34^+/CD45^-/CD146^+/CD133^+$; rCECs were $CD34^+/CD45^-/CD146^+/CD106^-$; and aCECs were $CD34^+/CD45^-/CD146^+/CD106^+$.

Flow cytometry was also used to assess the deposition of C3 and C5b-9 on HUVECs. Cells were incubated with fluorescein isothiocyanate (FITC)-conjugated anti-C3 antibody (Abcam, #ab4212) or anti-C5b-9 antibody (Abcam, #ab55811), followed by Alexa Fluor 647–conjugated goat anti-rabbit IgG H&L (Beyotime, #A0468). For HUVECs transduced with various lentiviral vectors, C5b-9 deposition was measured as above, whereas C3 deposition was detected using an APC-conjugated anti-C3 antibody (BioLegend, #846105).

Apoptosis was evaluated using the Annexin V-APC/7-AAD Apoptosis Kit (MultiSciences, #AP105) according to the manufacturer's instructions, followed by flow cytometric analysis.

Western blot analysis

Samples were subjected to immunoblotting using primary antibodies against human KLF4 (Abcam, #ab215036), CD46 (Abcam, #ab108307), C3 (Abcam, #ab181147), C5 (Proteintech, #66634-1-Ig), C4 (Proteintech, #22233-1-AP), CFB (Proteintech, #10170-1-AP), MBL2 (Invitrogen, #PA5-106674), C1QA (Proteintech, #67063-1-Ig) or β-actin (Proteintech, #66009-1-Ig), followed by corresponding species-specific secondary antibodies (Proteintech, #SA00001-1; Proteintech, #SA00001-2). This method enabled the assessment of protein levels for various complement components.

Quantitative real-time PCR

Quantitative real-time PCR (qPCR) was performed to assess the expression levels of various inflammatory and thrombotic endothelial genes, using primer sequences provided in Table S4. Relative gene expression was calculated using the comparative 2^-ΔΔCt method, normalized to the corresponding housekeeping gene.

Immunofluorescence staining

The cells treated with TA-TMA or control plasma were fixed with 4% paraformaldehyde PBS solution and permeabilized with 0.5% Triton X-100. After the cells were blocked with 10% normal goat serum for 1h, they were incubated with the same primary antibodies as in the Western blot analysis at 4°C overnight. Then they were stained with Alexa Fluor 647–conjugated goat anti-rabbit IgG H&L (Beyotime, #A0468) or Alexa Fluor 647 goat anti-

mouse IgG H&L (CST, #4410) for 2 h, followed by DAPI (Beyotime, #C1002) for 15 min at room temperature. Frozen mouse kidney sections were stained with anti-C3 (Abcam, #ab11862), anti-C5b-9 (Santa Cruz, #sc-66190), or anti-CD31 (Invitrogen, #PA5-32321) antibodies. Confocal images were acquired using a Leica inverted multiphoton laser scanning microscope. Immunofluorescence staining provides a direct visual representation of complement activation in cells and tissues.

Transendothelial electrical resistance and cell permeability

Cells were seeded onto 24-well Millicell inserts (pore size 0.4 μm, LABSELECT) and cultured until confluent. Transendothelial electrical resistance (TEER) was determined using a Millicell-ERS apparatus equipped with an electrode, and the change in resistance (ΔTEER) was calculated before and after plasma exposure, expressed as a percentage decrease from baseline. After 24h of plasma exposure, FITC-dextran (Sigma-Aldrich, #46944) was added to the apical chamber. Subsequently, 50 μL of medium from the lower chamber was transferred to a 96-well assay plate and its fluorescence intensity read at excitation/emission wavelengths of 485/540 nm using a BioTek plate reader.

CUT&Tag

CUT&Tag analysis was performed on KLF4-overexpressing HUVECs and control HUVECs, each exposed to TA-TMA plasma for 12 hours, by Jiayin Biotechnology Ltd. (Shanghai, China), following previously described protocols. Nuclei (5×10^5 per sample) were washed twice in wash buffer (20 mM HEPES, pH 7.5; 150 mM NaCl; 0.5 mM spermidine; 1 ×

protease-inhibitor cocktail). Each suspension was combined with 10 μL concanavalin A–coated magnetic beads (Bangs Laboratories) and incubated for 10 min at room temperature (RT). After removing unbound material, bead-bound nuclei were resuspended in DIG wash buffer (20 mM HEPES, pH 7.5; 150 mM NaCl; 0.5 mM spermidine; 1 × protease-inhibitor cocktail; 0.05% digitonin; 2 mM EDTA) and incubated overnight at 4°C with rotation with either anti-KLF4 antibody (Bio-Techne, #AF3640) or normal goat IgG (Bio-Techne, #AB-108-C). Following magnetic separation, nuclei were incubated for 60 min at RT with anti-goat IgG secondary antibody (Biodragon, #BF02015) diluted in DIG wash buffer. After three washes in DIG wash buffer, nuclei were incubated for 1 h at RT with a pA-Tn5 adapter complex (1:100) prepared in Dig-med buffer (20 mM HEPES, pH 7.5; 300 mM NaCl; 0.5 mM spermidine; 1 × protease-inhibitor cocktail; 0.01% digitonin). Samples were washed three times in Dig-med buffer, resuspended in tagmentation buffer (Dig-med + 10 mM $MgCl_2$), and tagmented for 1 h at 37°C. DNA was extracted by phenol–chloroform–isoamyl-alcohol and ethanol-precipitated, then PCR-amplified to generate sequencing libraries. Library size was verified on an Agilent 4200 TapeStation, and 150-bp paired-end sequencing was performed on an Illumina NovaSeq 6000. After quality control, reads were aligned to the reference genome with BWA, peaks were called with MACS2 ($q < 0.05$), annotated using ChIPseeker, and differential binding was assessed with DESeq2 ($|\text{fold-change}| \geq 2$, $p < 0.05$). Chromosomal distributions of KLF4 binding sites were visualized with the RIdeograms package.

To identify specific transcription factor binding sites within the promoter region of our gene

of interest, we first employed the 'Jaspar' package, which provides a comprehensive database of position weight matrices (PWMs) for diverse transcription factors [PMID: 37962376]. We extracted the genomic sequence corresponding to the upstream regulatory region and imported these sequences into Jaspar for motif scanning. This process yielded a set of putative KLF4-binding motifs, each associated with a predicted binding probability.

Subsequently, we utilized the 'Basenji' deep-learning framework to evaluate the functional significance of these potential regulatory elements. Basenji predicts gene expression by integrating long-range regulatory information through its multi-scale convolutional neural network architecture. Specifically, the model processes extended DNA sequences, often spanning tens to hundreds of kilobases, allowing it to capture enhancer–promoter interactions and distal regulatory cues that might influence transcriptional output [PMID: 32943643].

Within this computational platform, we performed in silico mutagenesis by systematically "knocking out" each putative KLF4-binding motif—replacing or removing the core nucleotides of the predicted site—while preserving the rest of the sequence context. Basenji then recomputed the predicted expression level for each altered sequence, providing a quantitative measure of the potential impact of each site's disruption. This step was crucial for identifying which motifs are most likely to contribute significantly to gene regulation.

By integrating the results from Jaspar motif identification with Basenji's predicted expression changes, we gained a clearer understanding of how KLF4 binding sites within the promoter region may shape transcriptional regulation and, ultimately, downstream biological processes.

RNA sequencing

Two distinct cell populations, hCECs and aHUVECs (n = 3 biological replicates per group), underwent total RNA extraction using a column-based purification kit, according to the manufacturer's guidelines. KLF4-overexpressing HUVECs and control HUVECs were each incubated with TA-TMA plasma for 12 hours (n = 3 per group), after which RNA-seq was performed. Library preparation, sequencing, and data analysis were carried out by Jiayin Biotechnology Ltd. (Shanghai, China), following previously described protocols. Differentially expressed genes (DEGs) were identified using the DESeq2 package ($|\text{fold change}| \geq 1.2$, $p < 0.05$). KEGG analysis was conducted, and the results were visualized using the OmicShare tool, an online data analysis platform.

Transfection and luciferase assays

Human CD46 reporter constructs were transfected into HEK 293T cells using FuGENE®6 Transfection Reagent (Promega, #E2691) according to the manufacturer's instructions. KLF4 or a control vector was co-transfected concurrently. A Renilla luciferase plasmid served as the internal control. After 48 hours, cells were lysed and analyzed with a luciferase assay (Promega, #E1910). The results were expressed as normalized fold

changes relative to controls. These luciferase assays verified the relationship between KLF4 expression and target gene transcription.

Animal treatment

Female 8-week-old C57BL/6J and BALB/C mice (Charles River Laboratories) were maintained in a specific-pathogen-free (SPF) facility at Soochow University.

To establish a hematopoietic stem cell transplantation model, BALB/C mice received a single lethal dose of total body X-ray irradiation (650 cGy) and were then transplanted with 1 times 10^7 C57BL/6J bone marrow cells via tail vein injection.[4]

To induce KLF4 expression, APTO-253 (MCE, #HY-16291) was administered by oral gavage twice daily at 5 mg/kg, dissolved in DMSO (Sigma-Aldrich, D4540), on post-transplant days +6, +8, +10, +12, and +14. Vehicle-treated animals received equivalent volumes of the solvent as controls.

We overexpressed KLF4 in vivo using a commercially available cationic polymer transfection reagent (in vivo-jetPEI®, Polyplus Transfection, #101000030). In brief, 30 μg of mKLF4 plasmid or the corresponding control vector (pcDNA3.1) was diluted in 200 μL of 5% glucose solution and mixed with in vivo-jetPEI® at the recommended ionic balance (N/P = 6-8). To achieve optimal KLF4 overexpression, the plasmid/ in vivo-jetPEI® mixture was administered via i.v. injection on days +12 and +14 post-transplantation to BALB/C

mice that had undergone allo-HSCT.

Pravastatin (20 mg/kg in 0.9% saline) was administered via oral gavage daily from post-transplantation days +8 to +14, while vehicle-treated groups received equivalent volumes of 0.9% saline through the same administration route and schedule during this period.

Then immunoblotting was performed on the kidney using an antibody against mouse KLF4 (Abcam, #ab214666) to validate its expression.

To reproduce TA-TMA pathology in vivo, we applied the dimethyloxalylglycine (DMOG) protocol previously optimized by our group.[2] Starting on day +15 after allo-HSCT, mice received daily intraperitoneal injections of DMOG (800 mg/kg; MCE, HY-15893) for two consecutive days, while control animals received equal volumes of 0.9% saline vehicle.

Statistics

Statistical analyses were conducted using GraphPad Prism 9.0 and SPSS 27.0 software. The Mann-Whitney *U* test (continuous variables) and chi-square test or Fisher's exact test (categorical variables) were used to estimate significant differences in baseline characteristics between the TA-TMA and control groups. Differences between two groups were evaluated using two-tailed Student's t-tests. For comparisons involving more than two groups, one-way analysis of variance (ANOVA) followed by Bonferroni's post-hoc test was employed. Survival incidence was assessed by the Kaplan-Meier method and the log-

rank test. Datas are described using mean ± standard deviation, while some datas are presented as median and interquartile range. A p-value < 0.05 was considered statistically significant.

References

1. Schoettler ML, Carreras E, Cho B, et al. Harmonizing Definitions for Diagnostic Criteria and Prognostic Assessment of Transplantation-Associated Thrombotic Microangiopathy: A Report on Behalf of the European Society for Blood and Marrow Transplantation, American Society for Transplantation and Cellular Therapy, Asia-Pacific Blood and Marrow Transplantation Group, and Center for International Blood and Marrow Transplant Research. Transplant Cell Ther 2023; 29(3): 151-163.

2. Qi J, Pan T, You T, et al. Upregulation of HIF-1α contributes to complement activation in transplantation-associated thrombotic microangiopathy. Br J Haematol 2022; 199(4): 603-615.

3. Zhou F, Zhou Y, Yang M, Wen J, Dong J, Tan W. Optimized multiparametric flow cytometric analysis of circulating endothelial cells and their subpopulations in peripheral blood of patients with solid tumors: a technical analysis. Cancer Manag Res 2018; 10: 447-464.

4. Cai Y, Ma S, Liu Y, et al. Adoptively transferred donor IL-17-producing CD4(+) T cells augment, but IL-17 alleviates, acute graft-versus-host disease. Cell Mol Immunol 2018; 15(3): 233-245.

Table S1 Clinical and laboratory parameters in TA-TMA patients and controls at sampling.

	Ctrl (n = 20)	TA-TMA (n = 20)	p-value
Median HGB, g/L (IQR)	92, 72.5-99.75	59, 52-69	< 0.0001
Median PLT, $\times 10^9$/L (IQR)	73.5, 43-117.5	12.5, 7-17.25	< 0.0001
Median LDH, U/L (IQR)	251.5, 208.0-339.0	654.0, 492.0-1076	< 0.0001
Median sC5b-9, ng/ml (IQR)	485.3, 443.0-564.3	1139, 754.1-1461	< 0.0001
rUPCR, n (%)			0.002
≥1 mg/mg	4 (20)	15 (75)	
<1 mg/mg	16 (80)	5 (25)	
Schistocytes, n (%)			< 0.001
Yes	1 (5)	12 (60)	
No	19 (95)	8 (40)	
Hypertension, n (%)			< 0.001
Yes	3 (15)	15 (75)	
No	17 (85)	5 (25)	

Abbreviations: HGB, hemoglobin; PLT, platelet; LDH, lactate dehydrogenase; rUPCR, random urine protein-to-creatinine ratio; IQR, interquartile range.

Table S2 Comparison of the numbers of CECs and their subpopulations in TA-TMA patients and controls.

Subpopulations	Ctrl (n = 10)	TA-TMA (n = 10)	p-value
Total cells	1×10^6	1×10^6	
mCECs (mean±standard deviation)	22.5 ± 7.706	88.5 ± 38.31	< 0.001
rCECs (mean±standard deviation)	24 ± 8.969	92.5 ± 40.24	< 0.001

Abbreviations: CECs, circulating endothelial cells; mCECs, mature ECs; rCECs, resting CECs.

Table S3 The predicted binding sites of KLF4 to CD46 as determined by CUT&Tag analysis

group	group_name	start	end	width	strand	score
1	NA	45	56	12	+	16.9044
1	NA	138	149	12	+	16.9044
2	NA	25	36	12	+	10.4034
2	NA	50	61	12	+	10.4034
3	NA	55	66	12	-	15.3195
3	NA	92	103	12	-	15.3195
3	NA	277	288	12	-	15.3195
4	NA	137	148	12	+	11.1982
5	NA	154	165	12	+	16.8562
6	NA	31	42	12	+	18.3429
6	NA	198	209	12	+	18.3429
7	NA	183	194	12	+	13.3239
8	NA	9	20	12	-	18.7868
9	NA	26	37	12	-	14.4497
10	NA	89	100	12	-	13.337
11	NA	11	22	12	+	10.7834
12	NA	100	111	12	+	18.0782
12	NA	309	320	12	+	18.0782
13	NA	169	180	12	+	15.1813
14	NA	55	66	12	+	7.28188
15	NA	290	301	12	-	17.268
16	NA	361	372	12	-	11.9243
16	NA	402	413	12	-	11.9243
17	NA	116	127	12	-	8.83229
18	NA	57	68	12	-	16.7749
19	NA	110	121	12	+	19.7101
20	NA	118	129	12	-	13.1542
21	NA	180	191	12	+	14.1056
22	NA	9	20	12	+	14.4222
23	NA	84	95	12	-	17.1012
24	NA	104	115	12	+	17.9629
25	NA	146	157	12	+	12.6989
26	NA	37	48	12	-	14.6597
27	NA	270	281	12	-	12.06
28	NA	179	190	12	-	16.2173
29	NA	249	260	12	+	18.2715
30	NA	72	83	12	-	17.2163
31	NA	179	190	12	-	13.8631
32	NA	55	66	12	+	17.2852
33	NA	225	236	12	+	16.4033
34	NA	173	184	12	+	17.704
35	NA	166	177	12	-	13.2508
36	NA	156	167	12	+	16.7067
37	NA	276	287	12	+	13.4827
38	NA	194	205	12	-	15.3495
39	NA	31	42	12	+	13.0741
40	NA	345	356	12	+	19.4453
41	NA	137	148	12	-	13.0267
42	NA	370	381	12	-	18.0782
43	NA	82	93	12	-	12.2288
44	NA	69	80	12	-	17.8694
45	NA	388	399	12	-	17.6981
46	NA	98	109	12	+	17.9128
47	NA	79	90	12	+	11.6202
48	NA	125	136	12	-	11.5453
49	NA	21	32	12	-	16.4033
50	NA	21	32	12	-	17.8694
51	NA	20	31	12	-	19.28

52	NA	41	52	12	-	17.8694
53	NA	54	65	12	-	11.7827
54	NA	31	42	12	+	16.6595
55	NA	17	28	12	+	18.0782
56	NA	73	84	12	-	15.4942
57	NA	16	27	12	+	17.9629
58	NA	101	112	12	-	18.5362
59	NA	4	15	12	-	9.85658
60	NA	36	47	12	-	16.1222
61	NA	102	113	12	+	14.8721
62	NA	179	190	12	-	13.9973
63	NA	75	86	12	+	12.446
64	NA	204	215	12	-	17.7204
65	NA	213	224	12	+	19.8254
66	NA	132	143	12	-	14.3932
67	NA	281	292	12	+	16.9052
68	NA	79	90	12	-	15.4119
69	NA	149	160	12	-	13.1082
70	NA	91	102	12	+	12.6069
71	NA	14	25	12	-	17.9629
71	NA	19	30	12	-	17.9629
72	NA	74	85	12	+	11.7078
73	NA	248	259	12	+	13.4533
74	NA	164	175	12	-	13.7287
75	NA	73	84	12	+	12.4342
76	NA	19	30	12	+	17.6481
77	NA	142	153	12	-	13.2277
78	NA	53	64	12	-	15.9592
79	NA	515	526	12	+	16.3782
80	NA	111	122	12	+	17.9629
80	NA	116	127	12	+	17.9629
81	NA	85	96	12	+	16.3948
82	NA	175	186	12	+	16.9044
83	NA	31	42	12	-	17.6981
83	NA	49	60	12	-	17.6981
83	NA	184	195	12	-	17.6981
83	NA	240	251	12	-	17.6981
84	NA	171	182	12	-	16.4761
85	NA	112	123	12	-	10.3143
86	NA	44	55	12	+	14.9002
87	NA	11	22	12	-	10.2666
88	NA	57	68	12	-	19.4453
89	NA	357	368	12	-	17.9629
90	NA	165	176	12	+	12.9305
91	NA	185	196	12	+	17.0396
92	NA	92	103	12	-	7.65363
93	NA	20	31	12	+	12.946
94	NA	55	66	12	-	18.5221
95	NA	185	196	12	-	11.3518
96	NA	48	59	12	+	15.3022
96	NA	211	222	12	+	15.3022
97	NA	309	320	12	-	17.6981
98	NA	78	89	12	+	8.7267
99	NA	258	269	12	-	17.8694
100	NA	134	145	12	+	10.9219
101	NA	206	217	12	-	16.5761
102	NA	24	35	12	-	17.2852
103	NA	289	300	12	-	11.9885
104	NA	121	132	12	-	11.5947
105	NA	23	34	12	-	16.668
106	NA	230	241	12	-	19.8254

107	NA	221	232	12	-	18.363
108	NA	4	15	12	-	13.7436
108	NA	44	55	12	-	13.7436
108	NA	84	95	12	-	13.7436
109	NA	14	25	12	-	16.92
110	NA	145	156	12	-	14.6762
111	NA	52	63	12	-	18.9163
112	NA	29	40	12	-	14.5707
113	NA	512	523	12	-	19.0152
114	NA	41	52	12	+	13.7385
115	NA	341	352	12	-	14.9595
116	NA	59	70	12	+	14.6795
117	NA	87	98	12	+	16.3541
118	NA	98	109	12	+	16.5243
119	NA	210	221	12	+	17.0596
120	NA	292	303	12	-	16.7119
121	NA	36	47	12	-	13.729
122	NA	194	205	12	+	14.5392
123	NA	15	26	12	+	10.8301
124	NA	274	285	12	+	11.7554
125	NA	123	134	12	-	17.1558
126	NA	172	183	12	+	18.1505
127	NA	97	108	12	-	17.5131
128	NA	117	128	12	+	18.0101
129	NA	142	153	12	+	13.2339
130	NA	5	16	12	-	19.8254
131	NA	94	105	12	-	18.9163
132	NA	23	34	12	+	16.7757
132	NA	79	90	12	+	16.7757
133	NA	247	258	12	+	11.0513
133	NA	295	306	12	+	11.0513
133	NA	395	406	12	+	11.0513
133	NA	421	432	12	+	11.0513
134	NA	5	16	12	+	9.30415
134	NA	31	42	12	+	9.30415
134	NA	55	66	12	+	9.30415
135	NA	175	186	12	+	17.6481
136	NA	268	279	12	-	18.0782
136	NA	352	363	12	-	18.0782
137	NA	6	17	12	+	18.3232
138	NA	82	93	12	-	19.3953
139	NA	49	60	12	-	17.8694
139	NA	218	229	12	-	17.8694
140	NA	576	587	12	+	16.6881
141	NA	44	55	12	-	18.0782
142	NA	193	204	12	-	18.142
143	NA	258	269	12	-	16.4899
144	NA	51	62	12	-	14.1003
145	NA	227	238	12	-	20.0901
146	NA	12	23	12	+	16.7119
147	NA	38	49	12	-	15.1
148	NA	150	161	12	+	16.8562
148	NA	33	44	12	-	16.8562
149	NA	199	210	12	-	13.8309
150	NA	4	15	12	-	18.5221
151	NA	51	62	12	+	12.5379
152	NA	21	32	12	+	11.2587
153	NA	12	23	12	-	15.129
154	NA	688	699	12	-	18.0782
155	NA	348	359	12	-	19.8254
156	NA	34	45	12	-	18.9163

157	NA	444	455	12	-	18.3429
157	NA	513	524	12	-	18.3429
158	NA	59	70	12	-	18.1341
158	NA	298	309	12	-	18.1341
159	NA	36	47	12	-	19.8254
160	NA	252	263	12	-	13.3511
161	NA	275	286	12	+	18.0782
162	NA	79	90	12	-	19.8254
163	NA	179	190	12	-	16.8562
164	NA	158	169	12	+	19.8254
165	NA	113	124	12	+	16.668
167	NA	138	149	12	+	8.07664
168	NA	108	119	12	-	8.52668
169	NA	235	246	12	+	18.363
170	NA	342	353	12	-	16.789
171	NA	130	141	12	-	18.0782
171	NA	162	173	12	-	18.0782
172	NA	147	158	12	-	16.8562
173	NA	163	174	12	+	18.0782
174	NA	150	161	12	-	13.2035
175	NA	17	28	12	-	18.1341
176	NA	31	42	12	-	18.3429
176	NA	112	123	12	-	18.3429
177	NA	227	238	12	-	18.0782
178	NA	48	59	12	+	13.3761
179	NA	286	297	12	-	16.9516
180	NA	254	265	12	-	18.3902
181	NA	173	184	12	+	17.0868
182	NA	335	346	12	+	17.8694
183	NA	5	16	12	+	16.4761
183	NA	249	260	12	+	16.4761
184	NA	102	113	12	-	17.3
185	NA	333	344	12	+	12.1125
186	NA	88	99	12	+	17.9629
187	NA	193	204	12	-	13.5992
188	NA	95	106	12	-	18.5362
189	NA	137	148	12	-	18.7868
190	NA	91	102	12	-	14.9507
191	NA	54	65	12	-	12.8836
192	NA	159	170	12	+	15.3022
193	NA	278	289	12	-	16.3511
194	NA	84	95	12	+	17.9629
195	NA	46	57	12	+	12.7743
195	NA	146	157	12	+	12.7743
196	NA	112	123	12	-	14.7971
197	NA	546	557	12	+	19.3953
198	NA	473	484	12	+	18.0782
199	NA	7	18	12	-	16.4033
200	NA	152	163	12	-	11.1474
201	NA	58	69	12	-	11.5631
202	NA	24	35	12	+	11.9322
203	NA	169	180	12	-	15.6823
204	NA	73	84	12	+	14.6544
205	NA	140	151	12	+	18.363
206	NA	169	180	12	-	13.3486
207	NA	549	560	12	-	15.1813
208	NA	47	58	12	-	14.1406
209	NA	108	119	12	+	16.4033
210	NA	22	33	12	+	18.0782
211	NA	54	65	12	+	12.2925
212	NA	67	78	12	-	11.7697

213	NA	50	61	12	+	13.0882
214	NA	251	262	12	+	16.8408
215	NA	63	74	12	-	16.3318
216	NA	111	122	12	+	12.714
217	NA	72	83	12	-	18.363
218	NA	149	160	12	-	12.7355
219	NA	248	259	12	+	15.1813
220	NA	92	103	12	+	15.1813
221	NA	104	115	12	-	9.36516
222	NA	249	260	12	+	14.1056
223	NA	9	20	12	-	12.507
224	NA	238	249	12	+	15.5528
225	NA	128	139	12	-	14.6272
226	NA	114	125	12	+	10.714
227	NA	63	74	12	-	16.0897
228	NA	186	197	12	-	16.4899
229	NA	12	23	12	+	15.0618
230	NA	96	107	12	-	17.7204
231	NA	63	74	12	-	13.7337
232	NA	419	430	12	+	17.1891
233	NA	84	95	12	+	9.48739
234	NA	23	34	12	-	18.0782
235	NA	44	55	12	+	12.9465
236	NA	72	83	12	-	17.9766
237	NA	171	182	12	-	12.2299
238	NA	497	508	12	+	17.8694
239	NA	105	116	12	-	18.5221
240	NA	267	278	12	-	18.4591
241	NA	5	16	12	-	10.9359
241	NA	74	85	12	-	10.9359
241	NA	147	158	12	-	10.9359
242	NA	135	146	12	-	14.9139
243	NA	78	89	12	-	17.4295
244	NA	223	234	12	+	16.789
245	NA	294	305	12	-	17.9629
246	NA	204	215	12	+	15.2294
247	NA	53	64	12	-	11.7533
248	NA	57	68	12	+	19.8254
249	NA	281	292	12	+	10.6528
250	NA	192	203	12	+	13.8257
251	NA	153	164	12	-	19.8254
252	NA	264	275	12	+	17.9629
253	NA	24	35	12	+	11.2743
254	NA	33	44	12	-	16.7757
255	NA	43	54	12	-	18.4591
256	NA	166	177	12	+	17.1891
257	NA	150	161	12	+	16.4341
258	NA	193	204	12	+	17.4295
259	NA	78	89	12	-	17.7932
260	NA	172	183	12	-	12.7419
261	NA	229	240	12	-	14.4222
262	NA	163	174	12	+	18.3429
263	NA	51	62	12	+	12.8142
264	NA	59	70	12	-	18.0782
265	NA	20	31	12	-	13.9973
266	NA	6	17	12	+	11.427
267	NA	152	163	12	-	17.0396
268	NA	5	16	12	+	8.52131
269	NA	172	183	12	-	15.1136
270	NA	141	152	12	-	11.5862
271	NA	43	54	12	+	16.9516

272	NA	162	173	12	+	14.3238
273	NA	126	137	12	-	12.8411
274	NA	247	258	12	+	18.0782
275	NA	156	167	12	+	13.0487
276	NA	32	43	12	+	18.142
277	NA	132	143	12	+	18.5362
278	NA	645	656	12	+	17.6481
279	NA	184	195	12	-	14.2471
280	NA	420	431	12	+	18.3232
281	NA	761	772	12	-	14.1336
282	NA	401	412	12	-	18.5362
283	NA	12	23	12	+	16.8408
284	NA	29	40	12	-	17.1691
284	NA	132	143	12	-	17.1691
285	NA	155	166	12	-	17.4295
286	NA	155	166	12	-	18.363
287	NA	89	100	12	+	16.7842
288	NA	29	40	12	+	14.6544
289	NA	157	168	12	+	12.6984
290	NA	303	314	12	-	11.8371
291	NA	253	264	12	+	17.1558
292	NA	127	138	12	+	13.6168
293	NA	341	352	12	+	18.0782
294	NA	159	170	12	+	14.9595
295	NA	9	20	12	-	16.4069
296	NA	133	144	12	+	18.0782
296	NA	174	185	12	+	18.0782
296	NA	257	268	12	+	18.0782
297	NA	313	324	12	-	17.268
298	NA	18	29	12	-	18.4067
299	NA	89	100	12	-	17.9629
300	NA	65	76	12	+	18.3567
301	NA	76	87	12	+	11.5521
302	NA	20	31	12	-	18.6515
303	NA	176	187	12	+	7.46487
304	NA	305	316	12	-	14.2128
305	NA	55	66	12	+	14.7279
306	NA	110	121	12	-	17.8694
307	NA	111	122	12	-	16.4743
308	NA	597	608	12	+	19.7101
309	NA	77	88	12	+	16.0897
310	NA	133	144	12	-	18.0782
310	NA	219	230	12	-	18.0782

Table S4 Primers used for real-time PCR

Species	Target name	Direction	Primer sequence
Human	*GAPDH*	Forward	GGAGCGAGATCCCTCCAAAAT
		Reverse	GGCTGTTGTCATACTTCTCATGG
	KLF4	Forward	CAGCTTCACCTATCCGATCCG
		Reverse	GACTCCCTGCCATAGAGGAGG
	ICAM-1	Forward	GGTAGCAGCCGCAGTCATAA
		Reverse	GATAGGTTCAGGGAGGCGTG
	VCAM-1	Forward	GGGAAGATGGTCGTGATCCTT
		Reverse	TCTGGGGTGGTCTCGATTTTA
	PAI-1	Forward	TGAGATCAGCACCACAGAC
		Reverse	ATTGATGATGAATCTGGCTCTC
	NOS3	Forward	GTGGCTGGTACATGAGCACT
		Reverse	TGGCTAGCTGGTAACTGTGC
	THBD	Forward	ACCTTCCTCAATGCCAGTCAG
		Reverse	CGTCGCCGTTCAGTAGCAA
Mouse	*Actb*	Forward	GTGACGTTGACATCCGTAAAGA
		Reverse	GCCGGACTCATCGTACTCC
	Icam-1	Forward	GTGATGCTCAGGTATCCATCCA
		Reverse	CACAGTTCTCAAAGCACAGCG
	Vcam-1	Forward	TGGTCGCGGTCTTGGGAGCCT
		Reverse	CCGGCTTCCCAACCTCCAGGGG
	Pai-1	Forward	GACACCCTCAGCATGTTCATC
		Reverse	AGGGTTGCACTAAACATGTCAG
	Vegfa	Forward	CTGGACCCTGGCTTTACTGC
		Reverse	CTGCTCTCCTTCTGTCGTGG
	Klf4	Forward	GAAGGTCGTGGCCCCGGAAA
		Reverse	TCAGTTCATCGGAGCGGGCG

Supplementary figure legends

Figure S1 | TA-TMA patients exhibit abnormal complement activation and endothelial injury.

A-C, C3b (A), C5b-9 (B), and KLF4 (C) levels across: TA-TMA patients (n = 20), controls (n = 20), acute graft-versus-host disease (aGVHD) patients (n = 10), and infection groups (n = 10).

D, Endothelial progenitor cells (EPCs) and mature circulating endothelial cells (mCECs) in peripheral blood in TA-TMA patients and controls are defined by flow cytometry. Bar graphs show the quantification of EPCs and mCECs. n = 10 per group.

E, Activated CECs (aCECs) and resting CECs (rCECs) in TA-TMA patients and controls are determined by flow cytometry and the bar graphs show the quantification of aCECs and rCECs. n = 10 per group.

**p < 0.01, ***p < 0.001, ****p < 0.0001. ns, not significant.

Figure S2 | Upregulation of KLF4 attenuates complement deposition and endothelial injury induced by TA-TMA plasma.

A, Complement C3 levels were determined by flow cytometry, and the bar graph shows fluorescence intensity of complement C3 on the HUVECs surface after incubation with plasma from control, infection, aGVHD and TA-TMA patients.

B, C, Flow cytometric analysis of C3 (B) and C5b-9 (C) deposition on HUVECs exposed to control plasma, TA-TMA plasma, or TA-TMA plasma supplemented with different concentrations of APTO253 (1 μM, 10 μM, 100 μM). Bar graphs show mean fluorescence

intensities.

D, Western blot shows enhanced KLF4 expression in HUVECs treated with 10 μM APTO253. Bar graph shows relative intensity of KLF4.

E, Western blot of C3, C5, C4, CFB, MBL2, and C1QA in HUVECs exposed to control plasma, TA-TMA plasma, or TA-TMA plasma supplemented with 10 μM APTO253. Bar graphs show relative protein levels.

F, Immunofluorescence staining of C3, C5b-9, C5, C4, CFB, MBL2, and C1QA in HUVECs under the same treatments. The bar graphs show mean fluorescence intensities. Scale bars: 50 μm.

G–K, qPCR analysis of *ICAM-1* (G), *VCAM-1* (H), *PAI-1* (I), *NOS3* (J), and *THBD* (K) in corresponding groups.

The results are representatives of three experiments. *p < 0.05, **p < 0.01, ***p < 0.001, ****p < 0.0001. ns, not significant.

Figure S3 | KLF4 overexpression reduces complement deposition and endothelial injury under TA-TMA plasma challenge.

A, Flow cytometric assessment of lentiviral transduction efficiency for control (PCDH) and KLF4-overexpressing (OEKLF4) vectors.

B, C, qPCR (B) and Western blot (C) confirming elevated KLF4 mRNA and protein levels in OEKLF4-transduced HUVECs.

D-F, Bar graphs compare the relative intensities of CFB (D), MBL2 (E) and C1QA (F) in PCDH and OEKLF4 cells treated with control or TA-TMA plasma.

G, Immunofluorescence analysis of the complement components (C3, C5b-9, C5, C4, CFB, MBL2, C1QA) in these cells. Scale bars: 50 μm.

H–L, Relative mRNA levels of *ICAM-1* (H), *VCAM-1* (I), *PAI-1* (J), *NOS3* (K), and *THBD* (L) determined by qPCR.

The results are representatives of three experiments. *p < 0.05, ** p < 0.01, ***p < 0.001, ****p < 0.0001. ns, not significant.

Figure S4 | KLF4 activates CD46 transcription in HUVECs.

A–D, KLF4-overexpressing (OEKLF4) and control lentiviral-transduced cells (PCDH) were incubated with TA-TMA plasma for 12 h and subjected to CUT&Tag assay with an anti-KLF4 antibody. A-B, the heatmap showed the distribution of KLF4 peaks in the vicinity of the translation start site (TSS). C, Annotation of KLF4 peaks on the genome. D, KEGG analysis of KLF4-enriched peaks in promoter regions.

E–G, RNA-seq analysis comparing OEKLF4 to PCDH cells under TA-TMA plasma for 12 h. E, Volcano plot of differentially expressed genes (DEGs). F, KEGG pathway analysis of upregulated genes. G, Overlap of CUT&Tag and RNA-seq data identifies potential KLF4 targets.

H, I, *CD46* mRNA levels measured by qPCR in OEKLF4 and PCDH cells exposed to acute graft-versus-host-disease plasma (H) and infection plasma (I). The results are representatives of three experiments.

J, Western blot validating stable CD46 knockdown (ShCD46) in HUVECs. The results are representatives of three experiments.

K-M, The bar graphs indicate the relative intensities of C4 (K), CFB (L) and MBL2 (M) in ShCD46 or control cells (PLKO.1) treated with control plasma, TA-TMA plasma, or TA-TMA plasma plus APTO253.

*p < 0.05, ** p < 0.01. ns, not significant.

Figure S5 | Upregulation of KLF4 attenuates the TA-TMA phenotype in mice.

A, Schematic timeline of APTO253 administration in the TA-TMA mouse model.

B, Western blot analysis of KLF4 levels in renal tissues from DMSO- and APTO253-treated mice. Bar graph shows relative intensity of KLF4. n = 4.

C, Hemoglobin (HGB) levels and platelet counts in mice treated with APTO253 or DMSO.

D, Representative peripheral blood smears (×100) showing fewer schistocytes (arrows) in the APTO253 group. Scale bars: 10 μm.

E–G, Plasma lactate dehydrogenase (LDH) (E), blood urea nitrogen (BUN) (F), and sC5b-9 (G).

H, Representative hematoxylin & eosin (H&E) and periodic acid–Schiff (PAS) staining highlighting improved glomerular architecture in the APTO253 group. Scale bar: 10 μm. Pound sign (#) indicates congestion; asterisk (★) indicates endothelial swelling/detachment.

I, Immunofluorescence of C3 and C5b-9 in renal sections. Bar graphs show mean fluorescence intensities. Scale bars: 10 μm.

J-M, qPCR quantification of *Icam-1* (J), *Vcam-1* (K), *Pai-1* (L), and *Vegfa* (M) in renal tissue. n = 4.

N-P, Plasma ICAM-1 (N), VCAM-1 (O), and PAI-1 (P).

Q, Kaplan–Meier survival curves for mice receiving different treatments.

The results are representatives of three experiments and six mice/group unless indicated.

*p < 0.05, **p < 0.01, ***p < 0.001, ****p < 0.0001. ns, not significant.

Figure S6 | In vivo KLF4 overexpression attenuates TA-TMA pathology.

A, Illustration of the protocol for KLF4 overexpression.

B, C, qPCR (B) and Western blot (C) analyses showing elevated KLF4 levels in renal tissues of mice receiving mKLF4 plasmids compared with vector controls. n = 4.

D-E, Plasma BUN (D) and sC5b-9 (E) in the indicated groups.

F-I, Relative mRNA levels of *Icam-1* (F), *Vcam-1* (G), *Pai-1* (H), and *Vegfa* (I) in renal tissue. n = 4.

J-L, Plasma levels of ICAM-1 (J), VCAM-1 (K), and PAI-1 (L).

The results are representatives of three experiments and six mice/group unless indicated.

*p < 0.05, **p < 0.01, ***p < 0.001, ****p < 0.0001.

Figure S7 | Statin treatment ameliorates TA-TMA by upregulating KLF4.

A, Timeline outlining pravastatin administration.

B, Western blot analysis of KLF4 levels in renal tissues from mice treated with pravastatin or vehicle. Bar graph shows relative intensity of KLF4. n = 4.

C-D, Plasma BUN (C) and sC5b-9 (D) in each group.

E-H, qPCR of *Icam-1* (E), *Vcam-1* (F), *Pai-1* (G), and *Vegfa* (H) in renal tissue. n = 4.

I-K, Plasma ICAM-1 (I), VCAM-1 (J), and PAI-1 (K) levels.

The results are representatives of three experiments and six mice/group unless indicated.

*$p < 0.05$, **$p < 0.01$, ***$p < 0.001$.

Figure S1

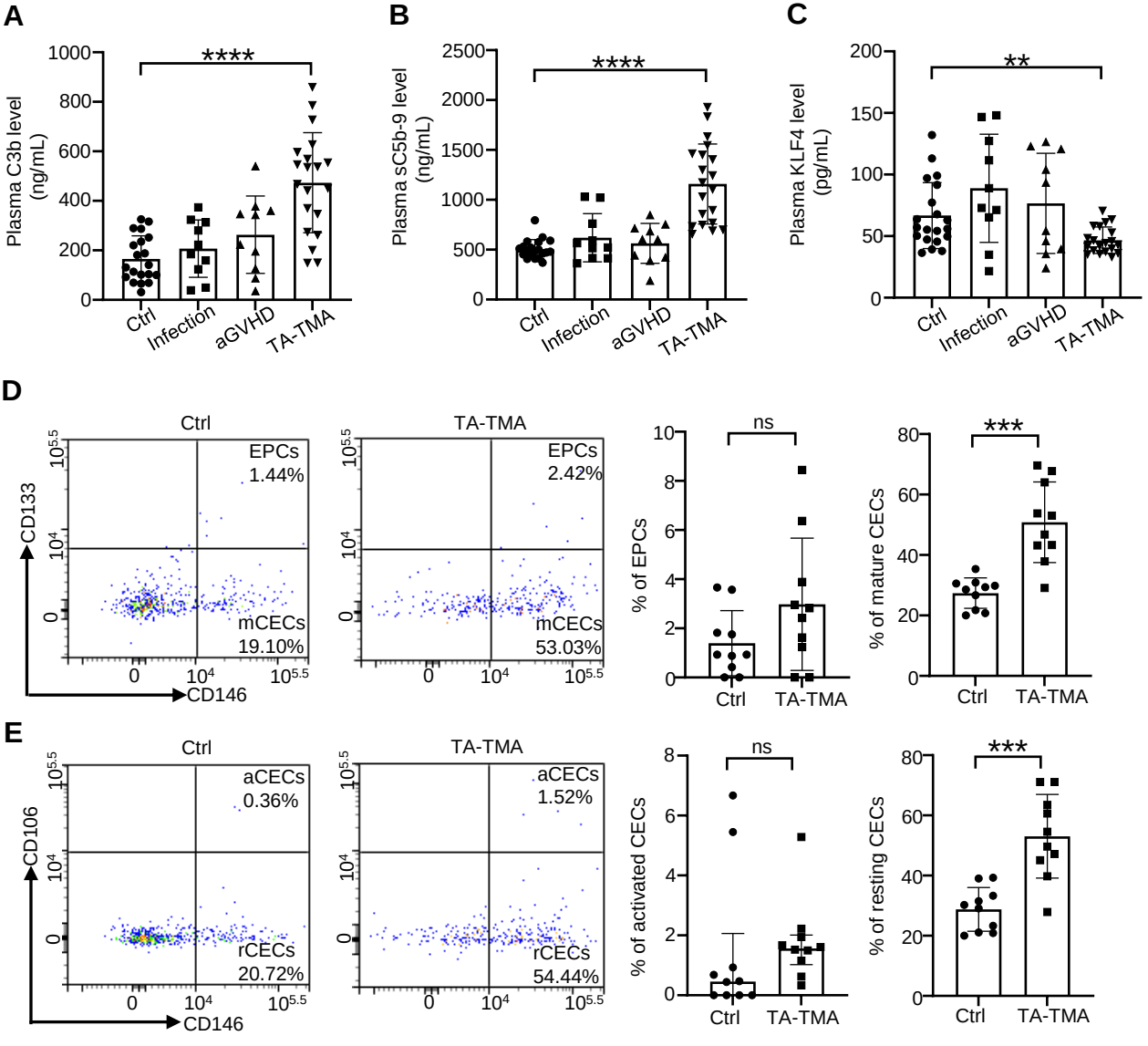
A
Plasma C3b level (ng/mL)
1000
800
600
400
200
0
****
Ctrl
Infection
aGVHD
TA-TMA
B
Plasma sC5b-9 level (ng/mL)
2500
2000
1500
1000
500
0
****
Ctrl
Infection
aGVHD
TA-TMA
C
Plasma KLF4 level (pg/mL)
200
150
100
50
0
**
Ctrl
Infection
aGVHD
TA-TMA
D
Ctrl
TA-TMA
CD133
CD146
EPCs
1.44%
mCECs
19.10%
EPCs
2.42%
mCECs
53.03%
ns
% of EPCs
***
% of mature CECs
E
Ctrl
TA-TMA
CD106
CD146
aCECs
0.36%
rCECs
20.72%
aCECs
1.52%
rCECs
54.44%
ns
% of activated CECs
***
% of resting CECs

Figure S2

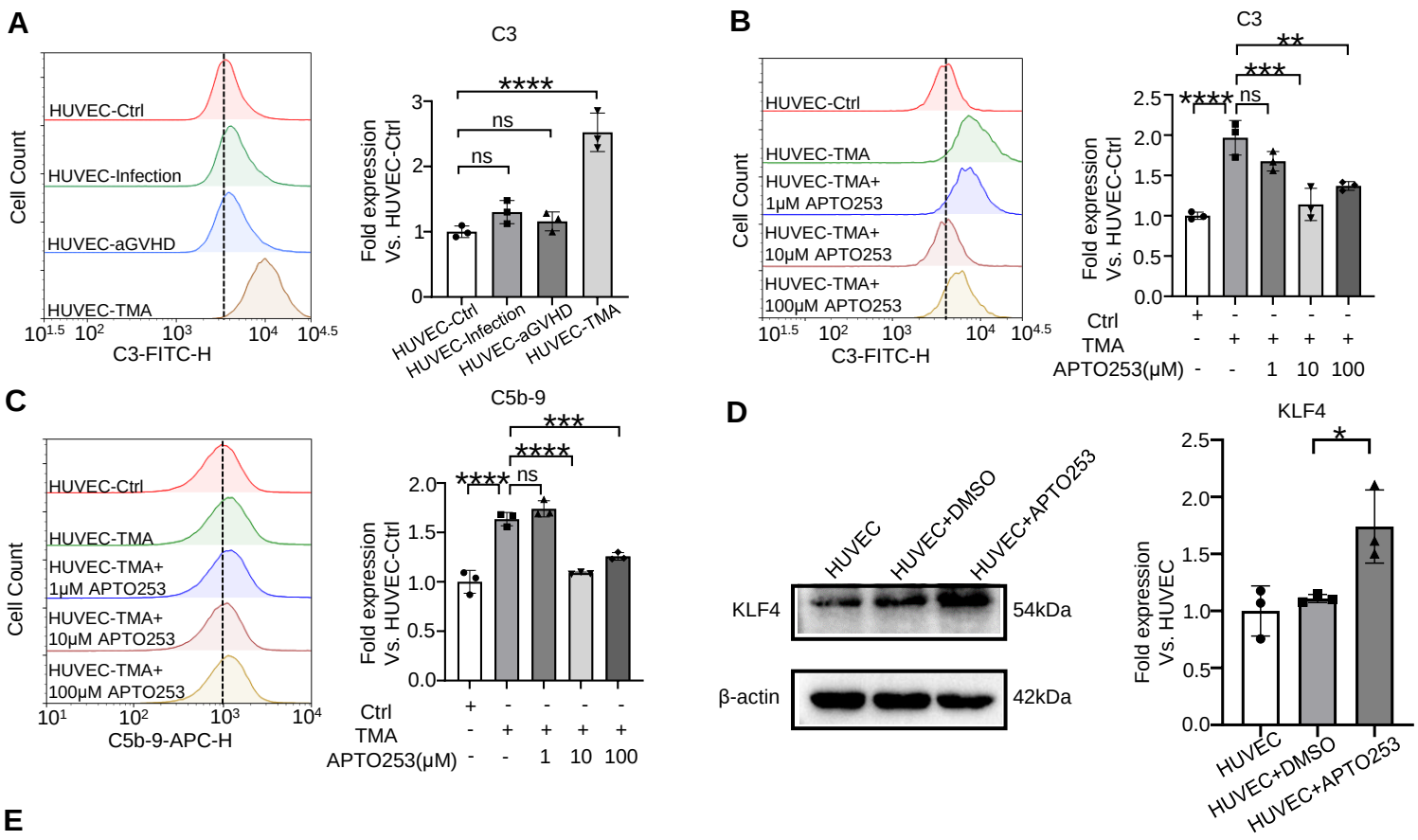
A
HUVEC-Ctrl
HUVEC-Infection
HUVEC-aGVHD
HUVEC-TMA
Cell Count
C3-FITC-H
C3
Fold expression Vs. HUVEC-Ctrl
B
HUVEC-TMA+ 1μM APTO253
HUVEC-TMA+ 10μM APTO253
HUVEC-TMA+ 100μM APTO253
Ctrl
TMA
APTO253(μM)
C
C5b-9
C5b-9-APC-H
D
HUVEC
HUVEC+DMSO
HUVEC+APTO253
KLF4
54kDa
β-actin
42kDa
E
C3
C5
C4
CFB
MBL2
C1QA
115kDa
85kDa
100kDa
32kDa
35kDa
42kDa
F
HUVEC-Ctrl
HUVEC-TMA
HUVEC-TMA +APTO253
DAPI/C3
DAPI/C5b-9
DAPI/C5
DAPI/C4
DAPI/CFB
DAPI/MBL2
DAPI/C1QA
Fold mean fluorescence intensity vs. HUVEC-Ctrl
G
ICAM-1 mRNA
H
VCAM-1 mRNA
I
PAI-1 mRNA
J
NOS3 mRNA
K
THBD mRNA

Figure S3

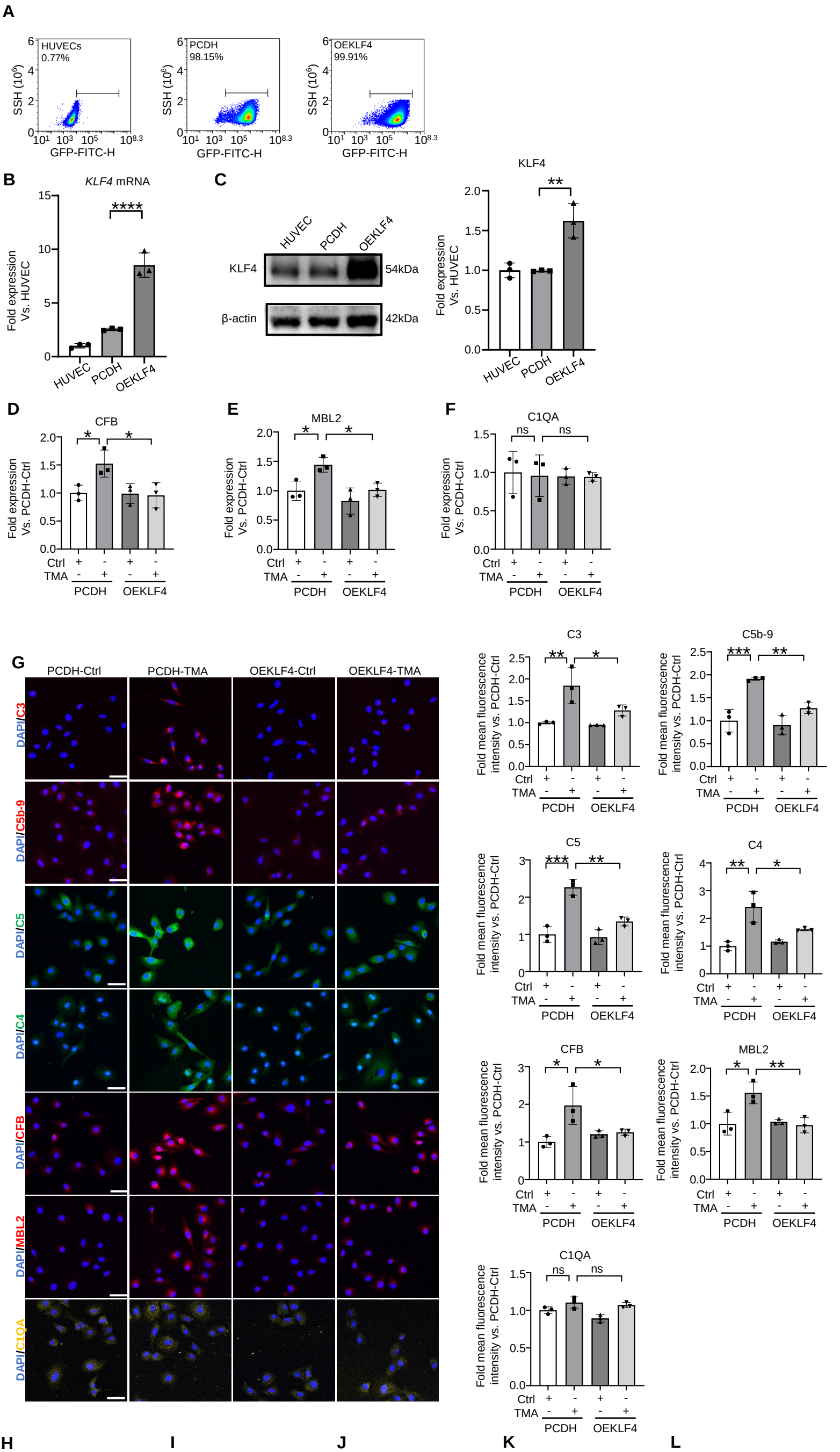
A
HUVECs
0.77%
PCDH
98.15%
OEKLF4
99.91%
SSH (10^6)
GFP-FITC-H
B
KLF4 mRNA
Fold expression Vs. HUVEC
HUVEC
PCDH
OEKLF4
C
KLF4
54kDa
β-actin
42kDa
D
CFB
E
MBL2
F
C1QA
Fold expression Vs. PCDH-Ctrl
Ctrl
TMA
G
PCDH-Ctrl
PCDH-TMA
OEKLF4-Ctrl
OEKLF4-TMA
DAPI/C3
DAPI/C5b-9
DAPI/C5
DAPI/C4
DAPI/CFB
DAPI/MBL2
DAPI/C1QA
Fold mean fluorescence intensity vs. PCDH-Ctrl
H
ICAM-1 mRNA
I
VCAM-1 mRNA
J
PAI-1 mRNA
K
NOS3 mRNA
L
THBD mRNA

Figure S4

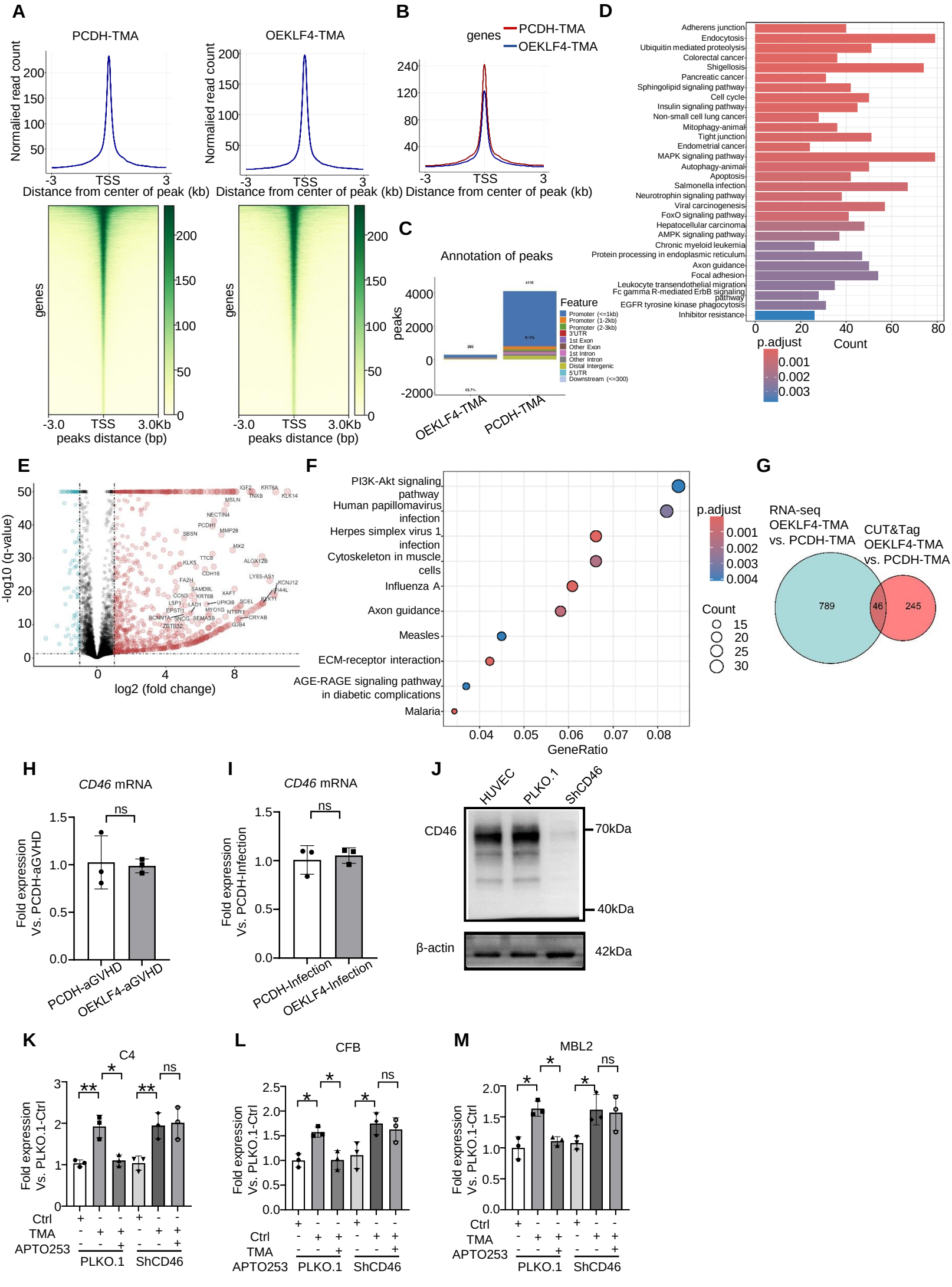
A
PCDH-TMA
OEKLF4-TMA
Normalied read count
Distance from center of peak (kb)
B
genes
PCDH-TMA
OEKLF4-TMA
C
Annotation of peaks
Feature
peaks
OEKLF4-TMA
PCDH-TMA
D
Adherens junction
Endocytosis
Ubiquitin mediated proteolysis
Colorectal cancer
Shigellosis
Pancreatic cancer
Sphingolipid signaling pathway
Cell cycle
Insulin signaling pathway
Non-small cell lung cancer
Mitophagy-animal
Tight junction
Endometrial cancer
MAPK signaling pathway
Autophagy-animal
Apoptosis
Salmonella infection
Neurotrophin signaling pathway
Viral carcinogenesis
FoxO signaling pathway
Hepatocellular carcinoma
AMPK signaling pathway
Chronic myeloid leukemia
Protein processing in endoplasmic reticulum
Axon guidance
Focal adhesion
Leukocyte transendothelial migration
Fc gamma R-mediated ErbB signaling pathway
EGFR tyrosine kinase phagocytosis
Inhibitor resistance
p.adjust
Count
E
-log10 (q-value)
log2 (fold change)
F
PI3K-Akt signaling pathway
Human papillomavirus infection
Herpes simplex virus 1 infection
Cytoskeleton in muscle cells
Influenza A
Axon guidance
Measles
ECM-receptor interaction
AGE-RAGE signaling pathway in diabetic complications
Malaria
GeneRatio
p.adjust
Count
G
RNA-seq
OEKLF4-TMA
vs. PCDH-TMA
CUT&Tag
OEKLF4-TMA
vs. PCDH-TMA
789
46
245
H
CD46 mRNA
Fold expression
Vs. PCDH-aGVHD
PCDH-aGVHD
OEKLF4-aGVHD
I
CD46 mRNA
Fold expression
Vs. PCDH-Infection
PCDH-Infection
OEKLF4-Infection
J
HUVEC
PLKO.1
ShCD46
CD46
70kDa
40kDa
β-actin
42kDa
K
C4
Fold expression
Vs. PLKO.1-Ctrl
Ctrl
TMA
APTO253
PLKO.1
ShCD46
L
CFB
M
MBL2

Figure S5

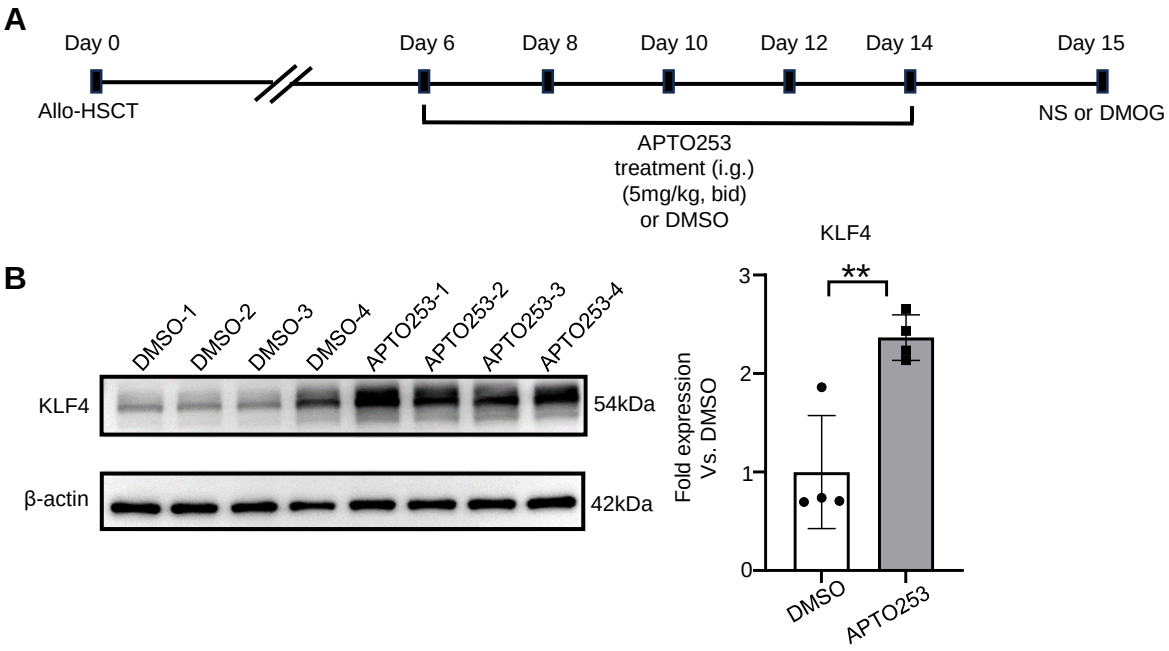
A
Day 0
Day 6
Day 8
Day 10
Day 12
Day 14
Day 15
Allo-HSCT
NS or DMOG
APTO253
treatment (i.g.)
(5mg/kg, bid)
or DMSO
B
DMSO-1
DMSO-2
DMSO-3
DMSO-4
APTO253-1
APTO253-2
APTO253-3
APTO253-4
KLF4
54kDa
β-actin
42kDa
KLF4
Fold expression
Vs. DMSO
DMSO
APTO253
C
HGB(*g/L)
PLT counts(*10^9/L)
Basline
Post-DMOG
Ctrl
DMOG+DMSO
DMOG+APTO253
D
Ctrl
DMOG+DMSO
DMOG+APTO253
E
LDH(U/L)
F
BUN(mg/dL)
G
Plasma sC5b-9 level
(ng/mL)
H
Ctrl
DMOG+DMSO
DMOG+APTO253
H&E
PAS
I
Ctrl
DMOG+DMSO
DMOG+APTO253
DAPI/CD31/C3
DAPI/CD31/C5b-9
C3
C5b-9
Fold mean fluorescence
intensity vs. Ctrl
J
Icam-1 mRNA
K
Vcam-1 mRNA
L
Pai-1 mRNA
Fold expression vs. Ctrl
M
Vegfa mRNA
N
Plasma ICAM-1 level (ng/mL)
O
Plasma VCAM-1 level (ng/mL)
P
Plasma PAI-1 level (ng/mL)
Q
Probability of Survival (100%)
Time (days)
p=0.11
Ctrl
DMOG+DMSO
DMOG+APTO253

Figure S6

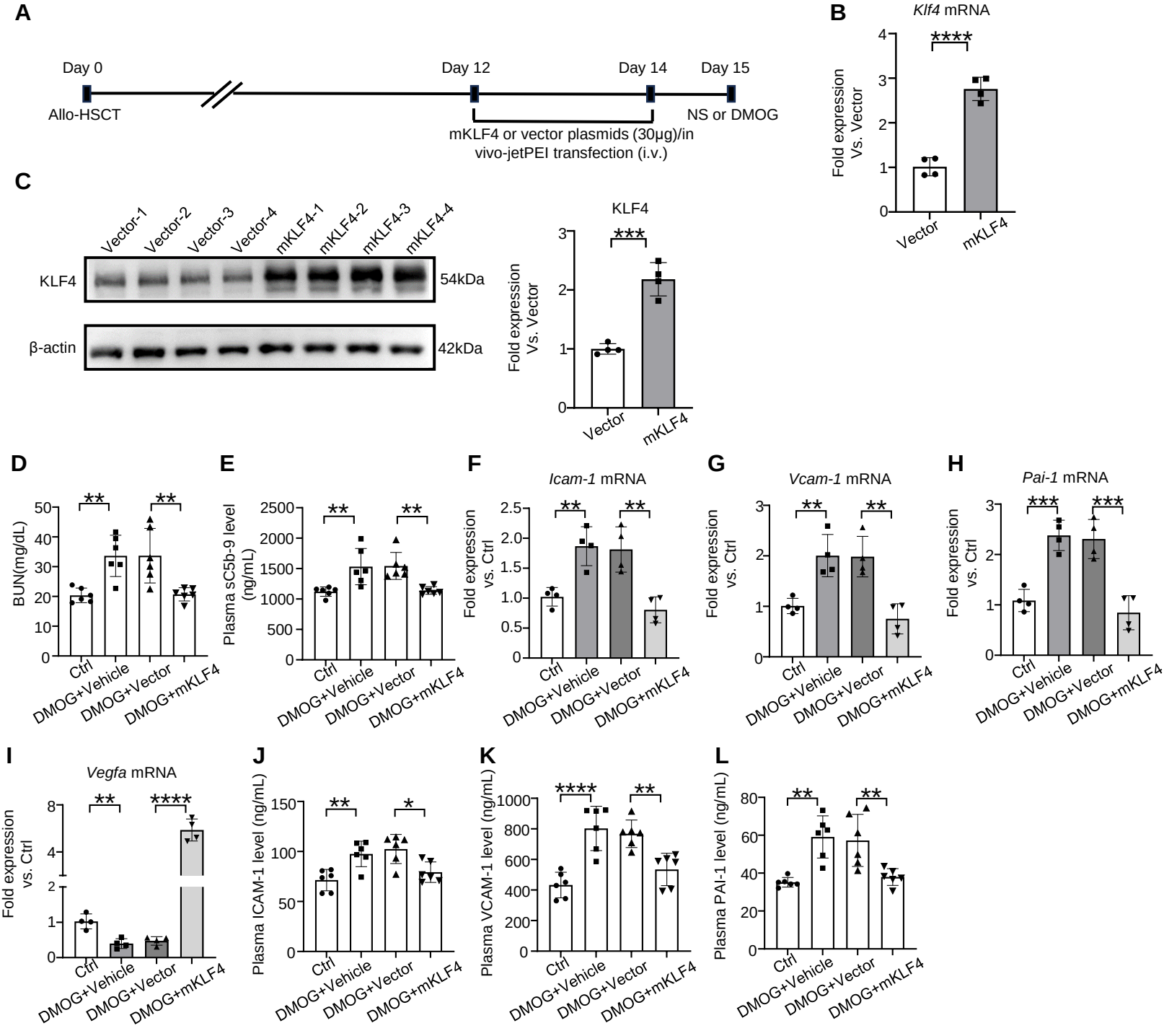
A
Day 0
Day 12
Day 14
Day 15
Allo-HSCT
NS or DMOG
mKLF4 or vector plasmids (30μg)/in vivo-jetPEI transfection (i.v.)
B
Klf4 mRNA
Fold expression Vs. Vector
Vector
mKLF4
C
Vector-1
Vector-2
Vector-3
Vector-4
mKLF4-1
mKLF4-2
mKLF4-3
mKLF4-4
KLF4
54kDa
β-actin
42kDa
KLF4
Fold expression Vs. Vector
D
BUN(mg/dL)
E
Plasma sC5b-9 level (ng/mL)
F
Icam-1 mRNA
Fold expression vs. Ctrl
G
Vcam-1 mRNA
H
Pai-1 mRNA
Ctrl
DMOG+Vehicle
DMOG+Vector
DMOG+mKLF4
I
Vegfa mRNA
J
Plasma ICAM-1 level (ng/mL)
K
Plasma VCAM-1 level (ng/mL)
L
Plasma PAI-1 level (ng/mL)

Figure S7

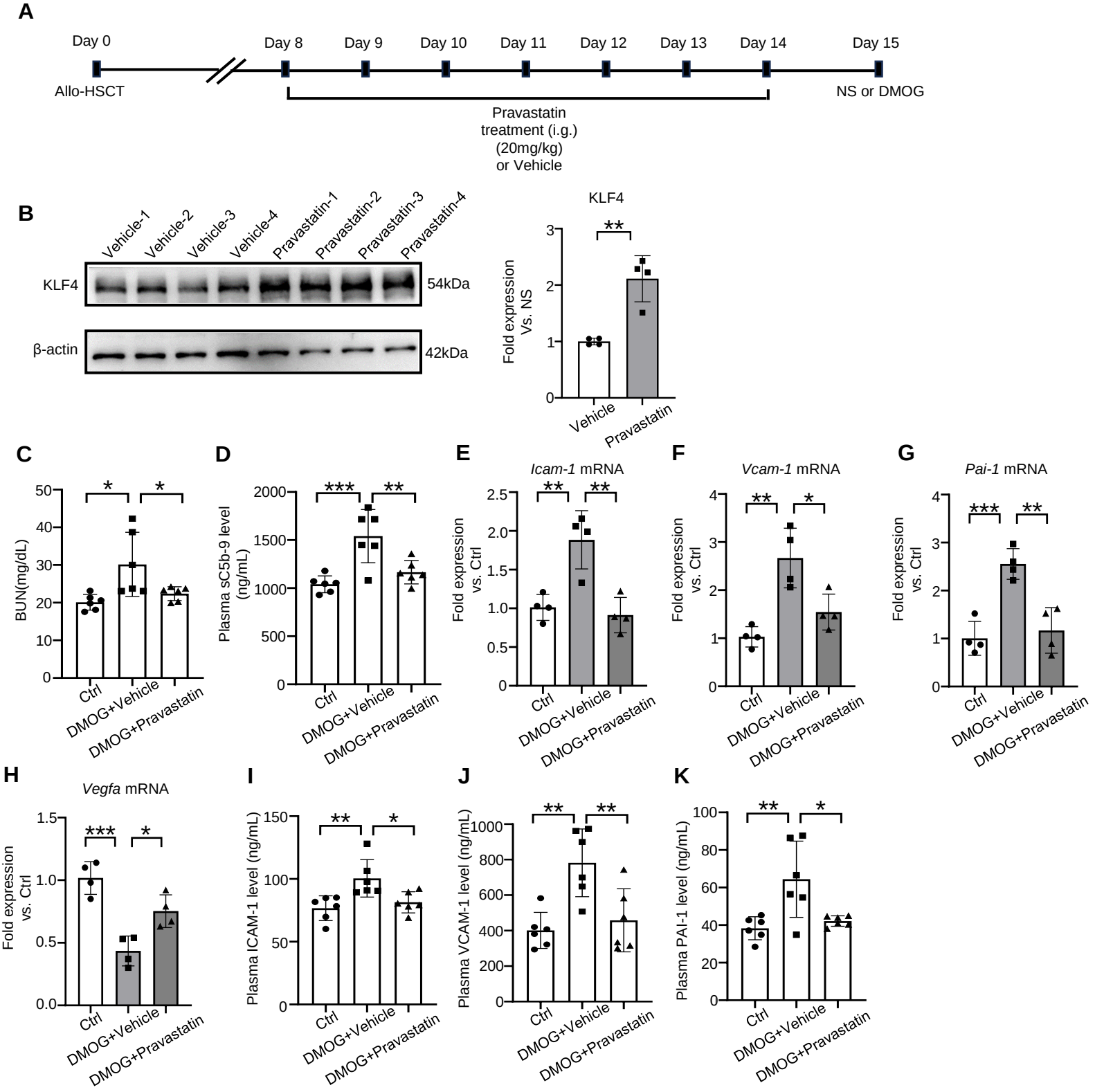
A
Day 0
Day 8
Day 9
Day 10
Day 11
Day 12
Day 13
Day 14
Day 15
Allo-HSCT
NS or DMOG
Pravastatin
treatment (i.g.)
(20mg/kg)
or Vehicle
B
Vehicle-1
Vehicle-2
Vehicle-3
Vehicle-4
Pravastatin-1
Pravastatin-2
Pravastatin-3
Pravastatin-4
KLF4
54kDa
β-actin
42kDa
KLF4
Fold expression
Vs. NS
Vehicle
Pravastatin
C
BUN(mg/dL)
D
Plasma sC5b-9 level
(ng/mL)
E
Icam-1 mRNA
Fold expression
vs. Ctrl
F
Vcam-1 mRNA
Fold expression
vs. Ctrl
G
Pai-1 mRNA
Fold expression
vs. Ctrl
Ctrl
DMOG+Vehicle
DMOG+Pravastatin
H
Vegfa mRNA
Fold expression
vs. Ctrl
I
Plasma ICAM-1 level (ng/mL)
J
Plasma VCAM-1 level (ng/mL)
K
Plasma PAI-1 level (ng/mL)